DERIVING LANDSCAPE-SCALE VEGETATION COVER AND ABOVEGROUND BIOMASS IN A SEMI-ARID ECOSYSTEM USING IMAGING SPECTROSCOPY

by

Andrew Poley

A thesis

submitted in partial fulfillment

of the requirements for the degree of

Master of Science in Geophysics

Boise State University

December 2017

BOISE STATE UNIVERSITY GRADUATE COLLEGE

DEFENSE COMMITTEE AND FINAL READING APPROVALS

of the thesis submitted by

Andrew Poley

Thesis Title: Deriving Landscape-Scale Vegetation Cover and Aboveground Biomass in a Semi-Arid Ecosystem Using Imaging Spectroscopy

Date of Final Oral Examination: 18 July 2017

The following individuals read and discussed the thesis submitted by student Andrew Poley, and they evaluated his presentation and response to questions during the final oral examination. They found that the student passed the final oral examination.

Nancy Glenn, Ph.D.	Chair, Supervisory Committee
Jennifer Forbey, Ph.D.	Member, Supervisory Committee
Dylan Mikesell, Ph.D.	Member, Supervisory Committee
Jennifer Pierce, Ph.D.	Member, Supervisory Committee

The final reading approval of the thesis was granted by Nancy F. Glenn, Ph.D., Chair of the Supervisory Committee. The thesis was approved by the Graduate College.

DEDICATION

Thank you to my advisor Dr. Nancy Glenn. Without your guidance, support, and patience this project would not have been possible. Thank you for being a great scientific role model. I would also like to thank Lucas Spaete for pushing me to test the limits of my abilities. A big shout out to the members of the Boise Center of Aerospace Laboratory. Thank you for your willingness to help me at any time and keeping me honest by constantly questioning my progress to ensure the integrity of the science. Finally I would like to thank my committee, Jennifer Pierce, Dylan Mikesell, and Jennifer Forbey. Thank you for your edits and support along the duration of this project.

ACKNOWLEDGEMENTS

Thank you to the NASA Terrestrial Ecology (NNX14AD81G) project for providing the funding that made this project possible. Thank you to United States Department of Agricultural Research Service Northwest Watershed Research Center and the Reynolds Creek Critical Zone Observatory (NSF EAR 1331872) for your services and support during the data collection portion of this project that took place at Reynold Creek Experimental Watershed. Thank you to the Boise State Geoscience Department for providing the necessary resources that allowed me to conduct this research.

ABSTRACT

Environmental disturbances in semi-arid ecosystems have highlighted the need to monitor current and future vegetation conditions across the landscape. Imaging spectroscopy provide the necessary information to derive vegetation characteristics at high-spatial resolutions across large geographic areas. The work of this thesis is divided into two sections focused on using imaging spectroscopy to estimate and classify vegetation cover, and approximate aboveground biomass in a semi-arid ecosystem.

The first half of this thesis assesses the ability of imaging spectroscopy to derive vegetation classes and their respective cover across large environmental gradients and ecotones often associated with semi-arid ecosystems. Optimal endmember selection and endmember bundling are coupled with classification and spectral unmixing techniques to derive vegetation species and abundances across Reynolds Creek Experimental Watershed (RCEW) in southwest Idaho at high spatial resolution (1 m). Results validated using field data indicated classification of aspen, Douglas fir, juniper, and riparian classes had an overall accuracy of 57.9% and a kappa coefficient of 0.43. Plant functional type classification, consisting of deciduous and evergreen trees, had an overall accuracy of 84.4% and a kappa coefficient of 0.68. Shrub, grass, and soil cover were predicted with an overall accuracy of 67.4% and kappa coefficient of 0.53. I conclude that imaging spectroscopy can be used to map vegetation communities in semi-arid ecosystems across large environmental gradients at high-spatial resolution and with high accuracy.

The second half of this thesis focuses on monitoring the changes of aboveground biomass (AGB) from the 2015 Soda Fire, which burned portions of southwest Idaho and southeastern Oregon. Classifications derived in the first study are used to estimate AGB loss within a portion of RCEW, and these estimates are used to compare to gross estimates made over the full extent of the Soda Fire. I found that there was an AGB loss of 174M kg within RCEW and approximately 1.8B kg lost over the full extent of the Soda Fire. Additionally, a post-fire analysis was performed to provide insight into the amount of AGB that returned to both RCEW and the full extent of the Soda Fire. An estimated 2,100 – 208,000 kg of AGB had returned to the burned portion of RCEW one-year post fire, and approximately 3.2M kg of AGB had returned over the full extent of the Soda Fire. These AGB loss and re-growth estimates can be used by researchers and practitioners to monitor carbon flux across the Soda Fire and as baseline data for wildfires in semi-arid ecosystems.

TABLE OF CONTENTS

LIST OF TABLES

LIST OF FIGURES

LIST OF EQUATIONS

LIST OF ABBREVIATIONS

AGB	Aboveground biomass
ALI	Advanced Land Imager
AVIRIS-ng	Airborne Visible/ Infrared Imaging Spectrometer next generation
BLM	Bureau of Land Management
CZO	Critical Zone Observatory
DEM	Digital Elevation Model
EAR	Endmember average root mean square error
EM	Endmember
ENVI	Environment for Visualizing Images
FIA	Forest Innovatory and Analysis
GB	Great Basin
GPS	Global Positioning System
LMM	Linear mixture model
MASA	Minimum average spectral angle
MESMA	Multispectral endmember spectral mixture analysis
MSAVI	Modified soil adjusted vegetation index
NAIP	National Agriculture Imagery Program
NIR	Near infrared
PA	Producer’s accuracy
PFT	Plant functional type

PV	Photosynthetic vegetation
RCEW	Reynolds Creek Experimental Watershed
RMSE	Root mean square error
RTK	Real time kinematic
SAM	Spectral angle mapper
SCM	Sub-pixel confusion-uncertainty matrix
SO3336	Sectorial Order 3336
TLS	Terrestrial laser scanner
UA	User's accuracy
USDA ARS	US Department of Agriculture Agricultural Research Service
VI	Vegetation index
VIPER	Visualization and Image Processing for Environmental Research

CHAPTER ONE: Introduction

1. Importance of work

Semi-arid ecosystems, defined by their scarcity of water, comprise over 40% (6B ha) of the world's total land surface, support 33% of the world's total population, and are important ecological and economic hotspots (Hassan, 2005). The Great Basin (GB), defined floristically as the extent of the sagebrush steppe, encompasses nearly 52M ha of the western United States (Figure 1-1) (Miller et al., 2013). Within the GB, elevation ranges from 400-3,000m, with average annual precipitation ranging from 150-300mm in lower elevation and 300-400mm in higher elevations (Miller et al., 2013). These large environmental gradients create transitions (ecotones) between different vegetation communities (biomes) across the landscape. A common ecotone within this landscape is the transition from the lower elevation sagebrush steppe to the higher elevation alpine forests. The sagebrush steppe is the most widespread biome in the USA, and has become the focus of current research as it supports many threatened species, contains important natural resources, and is vital to the country's economy (USFWS, 2014). Observing the sagebrush steppe vegetation, how it changes and co-exists with other biomes, and defining the biome's boundaries provides baseline information to monitor how the vegetation changes with time and disturbance. Furthermore, understanding fundamental changes in the sagebrush steppe can be used as an analog to understanding the rapid changes that are occurring in semi-arid ecosystems globally.

The spread of invasive grasses (Balch et al., 2012), expansion of woody trees (Romme et al., 2009), and an increase in drought severity (Yi et al., 2015), all influenced by current global climate changes, are connected to an increase in wildfire frequency, extent, and duration in the western USA. These environmental disturbances have led to both a fragmentation and loss of the native sagebrush steppe vegetation (Chambers et al., 2007; Miller et al., 2011; Bukowski and Baker, 2013), which has decreased regional carbon storage (Reichstein et al., 2013). Efforts made by government agencies in the past to restore semi-arid ecosystems after a fire disturbance have been extensive (Pyke 2011; Pyke et al., 2013; Nelson et al., 2014; Knutson et al., 2014). Research shows that pre-fire vegetation composition correlates to the effectiveness of these methods (Everett and Sharrow, 1985; Kuenzi et al., 2008; Boyd and Davies, 2010; Miller et al., 2013). However, historically there has been a lack of detailed landscape vegetation data available in semi-arid ecosystems to effectively adapt restoration efforts to semi-arid environments (Knick et al., 2003; Kiesecker et al., 2009; Mckenny and Kiesecker, 2009; Davies et al., 2011; Sanez et al., 2013). This lack of pre-fire vegetation data has led to the use of potentially ineffective restoration techniques, such as aerial and drill seeding, of shrub communities in the GB (Rafferty and Young, 2002; Boyd and Davies, 2010; Knutson et al., 2014; Barbec et al., 2015). As the landscape continues to diminish from wildfires, monitoring current vegetation conditions at the landscape scale becomes vital to enact effective restoration efforts.

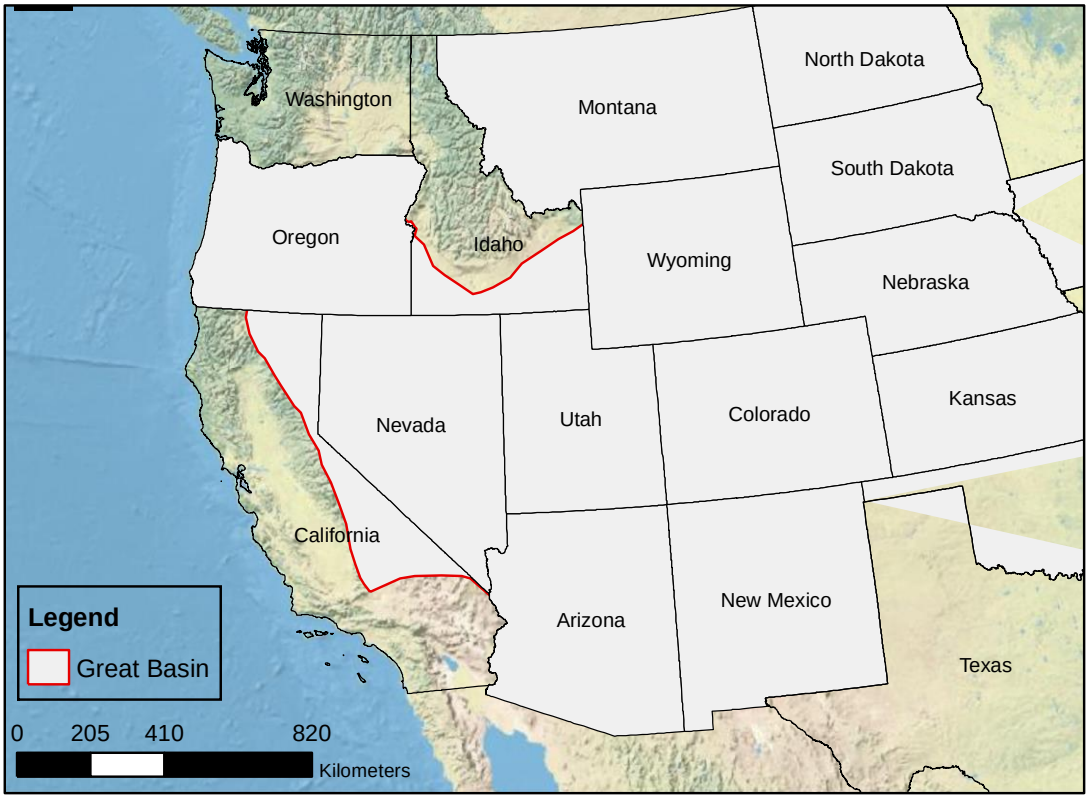

Figure 1-1: The extent of the Great Basin (GB) over the western United States. The GB is defined floristically as the extent of the sagebrush steppe.

The increasing concern regarding the environmental disturbances affecting vegetation in the GB has led to new public policies, land management practices, and wildlife protection strategies that aim to preserve the degrading landscape. Secretarial Order 3336 (SO3336) was established by the Secretary of the Interior on January 5th 2015. One of the goals of SO3335 is to advance technology to identify areas of high ecological and habitat value within the sagebrush steppe ecosystem. Furthermore, SO3336 aims to apply this knowledge to improve fire prevention methods, develop new long-term restoration techniques, and adapt management practices to improve land quality, reduce fuel loads, and protect wildlife. The goals of this policy stress the need to improve current vegetation classifications within the GB. In the past, landscape vegetation classifications in semi-arid ecosystems have been primarily produced using

medium to coarse-spatial resolution satellite imagery (30 m to 1 km spatial resolution). These data are often insufficient at capturing the heterogeneous vegetation patterns present, as sparse and fragmented shrub vegetation is masked by the large exposure of soil (Okin et al., 2001; Okin and Roberts, 2004). High spatial resolution vegetation classifications for semi-arid ecosystems are needed to improve our ability to monitor the changing vegetation conditions by providing insight into the landscape structure and functions necessary to establish restoration objectives at a range of different scales (Pyke, et al., 2015). In addition to improving post-fire restoration methods, high spatial resolution vegetation classifications will improve estimates of aboveground biomass (Eisfelder et al., 2012) and global carbon fluxes (Poulter et al., 2014). Specific to the GB, improving vegetation classification will support the objectives of SO3336, improve our ability to monitor degradation in the sagebrush steppe, and ultimately advance knowledge regarding the long-term sustainability of this ecosystem.

2. The 2015 Soda Fire

On August 10th, 2015, a lightning strike in Jordan Valley, Oregon, ignited the Soda Fire. The fire burned fairly continuous with a moderate to high burn severity across approximately 113,000 ha of sagebrush steppe landscape of government, state, and private lands in Oregon and Idaho before it was contained on August 23rd 2015. Restoration of the Soda Fire fell under SO3336 to fulfill the objective of rehabilitating degraded landscapes and mitigating the risk of future wildfires in the western United States. This fire is the first case study under SO3336 where post-fire effects threatening the degradation of the GB are identified to adapt and develop current methods to restore the landscape. Specific threats identified for the Soda Fire consist of expansion of

invasive species, habitat loss for threatened species, increased runoff leading to erosion and flooding, and loss of cultural resources. The SO3336 provided the funding to help target and eliminate these threats, and improve the sustainability of the GB.

The cost associated with the Soda Fire restoration efforts are estimated to be over $60M spent on wide application of a combination of different restoration methods over the burned area (Fritz et al., 2015). These methods consisted of aerial treatments of 9,000 ha of herbicide treatments, 25,000 ha of aerial seeding of shrubs, grasses and forbs, both native and introduced, 8,000 ha of drill seeding of native and introduced grasses, planting of approximately 1.35M sagebrush seedlings, and juniper removal in degraded areas unaffected by the fire for future fire repression (Fritz et al., 2015). Funding from the SO3336 also allowed the Bureau of Land Management (BLM) to develop new long-term ground monitoring protocols of the post-fire landscape. These protocols are being conducted to assess the effectiveness of the implemented restoration techniques. Assessment aims to determine if techniques are successful at minimizing threats to human life, property, and cultural resources, restoring habitats of threatened species, mitigating watershed responses and soil erosion, and reducing risk of future wildfires. Success of restoration methods developed for the Soda Fire will be important in helping fight the degradation of semi-arid ecosystems as wildfire frequency continues to increase in the GB.

3. Reynolds Creek Experiment Watershed

Reynolds Creek Experimental Watershed (RCEW) is located approximately 80 km southwest of Boise, Idaho, in the Owyhee Mountains, encompassing approximately 23,900 ha of semi-arid ecosystem. RCEW has an elevation gradient ranging from 900-

2100 m (Seyfried et al., 2000), and mean annual precipitation that varies from 250-1100 mm depending on elevation. Dominate shrub vegetation, primarily in the north, consists of Wyoming big sagebrush (*Artemisia tridentate ssp*.), low sagebrush (*Artemisia arbuscula*), and bitterbrush (*Pushia tridentate*), while dominate alpine vegetation in the south consists of quaking aspen (*Populus termuloides*) and Douglas fir (*Psuedotsuga menziesii*) (Seyfried et al., 2000). Juniper (Juniperus *occidentalis*) expansion has also been noted in the transitional zones of the watershed (Sankey at al., 2010). Supported by the USDA Agriculture Research Service Northwest Watershed Research Center, RCEW is a well-studied area by researchers across many fields (e.g., ecology, geomorphology, hydrology, geophysics, etc.) resulting in the availability of robust and diverse datasets. Recently, RCEW has become part of the National Science Foundation's Critical Zone Observatory program (CZO, NSF EAR 1331872).

In the summer of 2015, approximately 7,300 ha of the northern portion of RCEW (~1/3 of the total watershed) was burned during the Soda Fire. This area burned at a high burn severity, incinerating most all vegetation. A majority of this area was treated with restoration efforts as part of SO3336. Remote sensing and field data collected prior to the Soda Fire within the watershed serve as an opportunity to study ecosystem changes from the fire and the effectiveness of restoration techniques by providing detailed landscape information about the pre-fire vegetation conditions. Knowledge gained from restoration efforts in RCEW is beneficial for adapting future restoration efforts of other post-fire areas within the GB under the direction of SO3336, and will provide insight for restoration efforts in semi-arid ecosystems worldwide.

4. Thesis organization

My thesis is divided into a background section defining imaging spectroscopy and spectral mixing, two self-contained manuscripts, and a conclusion section highlighting the major findings of this work. The first manuscript explores the use of imaging spectroscopy to classify vegetation across multiple biomes and ecotones within RCEW. Classifications are derived at very high spatial resolutions (1 m) and serve as a reference state of the current vegetation conditions present within RCEW. This information can be used in turn to track changes in vegetation compositions and well as paired with any number of other scientific studies (e.g. hydrologic modeling) in RCEW. The second manuscript is a case study focusing on the changes in aboveground biomass that occurred from the 2015 Soda Fire. This chapter provides gross estimates of the aboveground biomass lost within RCEW and over the full extent of the Soda Fire. Finally, an initial assessment of how much aboveground biomass has returned one-year following the wildfire both within RCEW and over the full extent of the Soda Fire is presented.

5. References

Brabec, M. M., Germino, M. J., Shinneman, D. J., Pilliod, D. S., Mcilroy, S. K., & Arkle, R. S. (2015). Challenges of Establishing Big Sagebrush (Artemisia tridentata) in Rangeland Restoration: Effects of Herbicide, Mowing, Whole-Community Seeding, and Sagebrush Seed Sources. *Rangeland Ecology & Management,68*(5), 432-435. doi:10.1016/j.rama.2015.07.001

Balch, J. K., Bradley, B. A., Dantonio, C. M., & Gómez-Dans, J. (2012). Introduced annual grass increases regional fire activity across the arid western USA (1980-2009). *Global Change Biology, 19*(1), 173-183. doi:10.1111/gcb.12046

Boyd, C. S., & Davies, K. W. (2010). Shrub Microsite Influences Post-Fire Perennial Grass Establishment. *Rangeland Ecology & Management, 63*(2), 248-252. doi:10.2111/rem-d-09-00025.1

Bukowski, B. E., & Baker, W. L. (2013). Historical fire regimes, reconstructed from land-survey data, led to complexity and fluctuation in sagebrush landscapes. *Ecological Applications, 23*(3), 546-564. doi:10.1890/12-0844.1

Chambers, J. C., Roundy, B. A., Blank, R. R., Meyer, S. E., & Whittaker, A. (2007). What Makes Great Basin Sagebrush Ecosystems Invasible Bybromus Tectorum? *Ecological Monographs, 77*(1), 117-145. doi:10.1890/05-1991

Davies, K. W., Boyd, C. S., Beck, J. L., Bates, J. D., Svejcar, T. J., & Gregg, M. A. (2011). Saving the sagebrush sea: An ecosystem conservation plan for big sagebrush plant communities. *Biological Conservation, 144*(11), 2573-2584. doi:10.1016/j.biocon.2011.07.016

Eisfelder, C., Kuenzer, C., & Dech, S. (2012). Derivation of biomass information for semi-arid areas using remote-sensing data. *International Journal of Remote Sensing, 33*(9), 2937-2984. doi:10.1080/01431161.2011.620034

Everett, R. L., & Sharrow, S. H. (1985). Response of grass species to tree harvesting in single leaf pinyon-Utah juniper stands /. doi:10.5962/bhl.title.69006

Fritz, C., Webb, A., Bennett, R., Stillman, A., Meier, H., & Ashby, C. (2015). BLM Idaho Post-Fire Recovery Plan Emergency Stabilization and Burned are Rehabilitation 2015 Plan. *J08B SODA.*

Hassan, R. (2005). *Ecosystems and human well-being*. Washington, D.C.: Island Press.

Kiesecker, J. M., Copeland, H., Pocewicz, A., Nibbelink, N., Mckenney, B., Dahlke, J., & Stroud, D. (2009). A Framework for Implementing Biodiversity Offsets: Selecting Sites and Determining Scale. *BioScience, 59*(1), 77-84. doi:10.1525/bio.2009.59.1.11

Knick, S. T., Dobkin, D. S., Rotenberry, J. T., Schroeder, M. A., Haegen, W. M., & Riper, C. V. (2003). Teetering On The Edge Or Too Late? Conservation And

Research Issues For Avifauna Of Sagebrush Habitats. *The Condor, 105*(4), 611. doi:10.1650/7329

Knutson, K. C., Pyke, D. A., Wirth, T. A., Arkle, R. S., Pilliod, D. S., Brooks, M. L., & Grace, J. B. (2014). Long-term effects of seeding after wildfire on vegetation in Great Basin shrubland ecosystems. *Journal of Applied Ecology,51*(5), 1414-1424. doi:10.1111/1365- 2664.12309

Kuenzi, A. M., Fulé, P. Z., & Sieg, C. H. (2008). Effects of fire severity and pre-fire stand treatment on plant community recovery after a large wildfire. *Forest Ecology and Management, 255*(3-4), 855-865. doi:10.1016/j.foreco.2007.10.001

Mckenney, B. A., & Kiesecker, J. M. (2009). Policy Development for Biodiversity Offsets: A Review of Offset Frameworks. *Environmental Management, 45*(1), 165-176. doi:10.1007/s00267-009-9396-3

Miller, R. F., Knick, S. T., Pyke, D. A., Meinke, C. W., Hanser, S. E., Wisdom, M. J., & Hild, A. L. (2011). Characteristics of Sagebrush Habitats and Limitations to Long-Term Conservation. *Greater Sage-GrouseEcology and Conservation of a Landscape Species and Its Habitats*, 144-184. doi:10.1525/california/9780520267114.003.0011

Miller, R. F., Chambers, J. C., Pyke, D. A., Pierson, F. B., & Williams, C. J. (2013). A review of fire effects on vegetation and soils in the Great Basin Region: response and ecological site characteristics. doi:10.2737/rmrs-gtr-308

Nelson, Z. J., Weisberg, P. J., & Kitchen, S. G. (2014). Influence of climate and environment on post-fire recovery of mountain big sagebrush. *International Journal of Wildland Fire, 23*(1), 131. doi:10.1071/wf13012

Okin, G. S., Roberts, D. A., Murray, B., & Okin, W. J. (2001). Practical limits on hyperspectral vegetation discrimination in arid and semiarid environments. *Remote Sensing of Environment, 77*(2), 212-225. doi:10.1016/s0034-4257(01)00207-3

Okin, G. S., & Roberts, D. A. (2004). Remote sensing in arid regions: challenges and oppurtunities.

Poulter, B., Frank, D., Ciais, P., Myneni, R. B., Andela, N., Bi, J., & Werf, G. R. (2014). Contribution of semi-arid ecosystems to interannual variability of the global carbon cycle. *Nature, 509*(7502), 600-603. doi:10.1038/nature13376

Pyke, D. A. (2011). Restoring and Rehabilitating Sagebrush Habitats. *Greater Sage-GrouseEcology and Conservation of a Landscape Species and Its Habitats,* 530-548. doi:10.1525/california/9780520267114.003.0024

Pyke, D. A., Wirth, T. A., & Beyers, J. L. (2013). Does Seeding After Wildfires in Rangelands Reduce Erosion or Invasive Species? *Restoration Ecology*, *21*(4), 415-421. doi:10.1111/rec.12021

Pyke, D. A., Chambers, J. C., Pellant, M., Knick, S. T., Miller, R. F., Beck, J. L., & Mciver, J. D. (2015). Restoration handbook for sagebrush steppe ecosystems with emphasis on greater sage-grouse habitat—Part 1. Concepts for understanding and applying restoration. *Circular*. doi:10.3133/cir1416

Rafferty, D., & Young, J. (2002). Cheatgrass competition and establishment of desert needlegrass seedlings. *Journal of Range Management, 55*(1). doi:10.2458/azu_jrm_v55i1_rafferty

Reichstein, M., Bahn, M., Ciais, P., Frank, D., Mahecha, M. D., Seneviratne, S. I., & Wattenbach, M. (2013). Climate extremes and the carbon cycle. *Nature, 500*(7462), 287-295. doi:10.1038/nature12350

Romme, W. H., Allen, C. D., Bailey, J. D., Baker, W. L., Bestelmeyer, B. T., Brown, P. M., & Weisberg, P. J. (2009). Historical and Modern Disturbance Regimes, Stand Structures, and Landscape Dynamics in Piñon–Juniper Vegetation of the Western United States. *Rangeland Ecology & Management, 62*(3), 203-222. doi:10.2111/08-188r1.1

Saenz, S., Walschburger, T., González, J. C., León, J., Mckenney, B., & Kiesecker, J. (2013). Development by Design in Colombia: Making Mitigation Decisions Consistent with Conservation Outcomes. *PLoS ONE, 8*(12). doi:10.1371/journal.pone.0081831

Sankey, T. T., Glenn, N., Ehinger, S., Boehm, A., & Hardegree, S. (2010). Characterizing Western Juniper Expansion via a Fusion of Landsat 5 Thematic Mapper and Lidar Data. *Rangeland Ecology & Management, 63*(5), 514-523. doi:10.2111/rem-d-09-00181.1

Seyfried, M. S., Harris, R. C., Marks, D., & Jacob, B. (2000). A geographic database for watershed research, Reynolds Creek Experimental Watershed, Idaho, USA. *Tech. Bull. NWRC 2000*, *3*, 26.

U.S. Fish Wildlife Service Why Care About America's Sagebrush? (2014).

Yi, C., Pendall, E., & Ciais, P. (2015). Focus on extreme events and the carbon cycle. *Environmental Research Letters, 10*(7), 070201. doi:10.1088/1748-9326/10/7/070201

CHAPTER TWO: BACKGROUND

Imaging spectroscopy

Imaging spectroscopy, or hyperspectral imaging, is the use of hundreds of nanometer-sized channels to observe the spectral properties of objects from the visible to shortwave-infrared (400-2500 nm) portions of the electromagnetic spectrum (Figure 2-2). The high spectral resolution of hyperspectral sensors, such as NASA's Airborne Visible/ Infrared Imaging Spectrometer- next generation (AVIRIS-ng), can be used to extract spectral information from an object that traditional broadband multispectral sensors, such as Landsat, cannot. Previous studies have determined the advantages of using hyperspectral imagery over multispectral imaging, which include the ability to map invasive vegetation species (Underwood et al., 2003; Lawrence et al., 2006), identify vegetation species (Ghiyamat et al., 2013; Ballanti et al., 2016), and estimate vegetation abundances (Roberts et al., 1993; Asner and Heidebrecht, 2002; Roth et al., 2015). Hyperspectral imagery's ability to capture this detailed spectral information of vegetation is crucial in studying semi-arid ecosystems where the heterogeneity of the landscape, spectral similarity between vegetation species, and high soil albedo often mask the sparse vegetation in remote sensing data (Okin et al., 2001; Okin and Roberts, 2004).

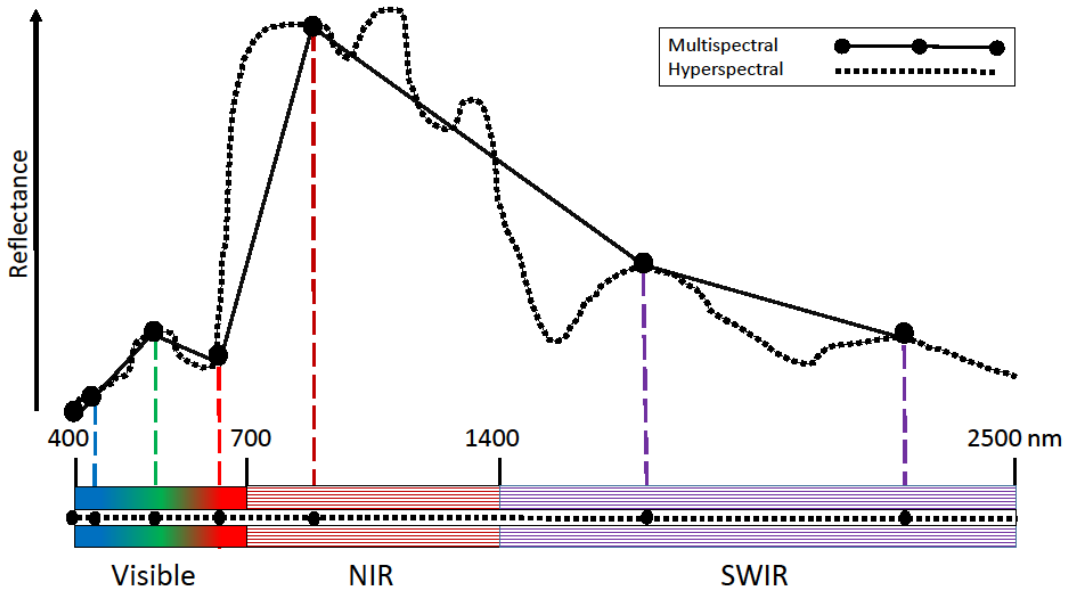

Figure 2-1: Multispectral imagery (large dots) collects spectral information only at several locations across the electromagnetic spectrum. Hyperspectral imagery (small dots) collects spectral information at discrete intervals and is able to better capture spectral information of objects.

Spectral mixing

Spectral mixing is the processes of recording the combination of reflected radiation from multiple materials on Earth's surface by an imaging spectrometer. There are two types of mixing that can affect radiation before it reaches the sensor: linear and nonlinear mixing. Linear mixing assumes incoming radiation from several materials remains separated until it reaches the sensor where it is then added together due to the lower spectral resolution of the sensor (Figure 2-1) (Campbell and Wynne, 2011). Nonlinear mixing occurs when reflected radiation from multiple materials interacts on the surface before being recorded by the sensor (Figure 2-1) (Campbell and Wynne, 2011). Nonlinear mixing is much more likely to occur due to the complex structure of Earth's surface, especially in heterogeneous landscapes such as semi-arid ecosystems. However, decomposing this nonlinear spectral information into its respective parts is challenging

because it often requires detailed knowledge of the surface cover and the use of physics-based models (Heylen et al., 2014). It has been found that the assumptions of linear mixing models are often sufficient to approximate the effects of spectral mixing (Qin and Gerstl, 2000; Keshava and Mustard, 2002; Bioucas-Dias et al., 2012).

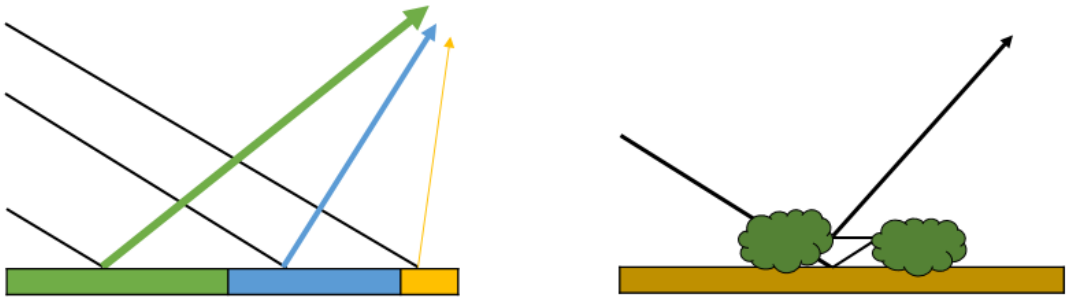

Figure 2-3: Linear spectral mixing (left) uses the assumption that the ground is divided into sections that are proportional to their contributing reflectance. Nonlinear spectral mixing (right) occurs when radiation interacts between objects at the surface before being reflected and recorded by the sensor.

Image classification

Image classification is the process of extracting information from an image by relating its spectral or spatial information to real-world physical classes. Spectral image classification compares the known unique spectral properties of a material, termed endmembers (EM), to a pixel spectrum and identifies that pixel as the EM that it most resembles. Previous studies have performed this type of image classification in semi-arid ecosystems to perform landcover classification (Roth et al., 2015), detect invasive species (Glenn et al., 2005), and calculate the burn extent of a wildfire (Eckmann et al., 2009). Image classification of spectral data can be divided into two methods: hard and soft image classification. Hard image classification is the process of assigning each pixel in a remotely sensed imaged to a single class or category (Figure 2-3). Hard image

classification is useful when the classes being classified are coarser than the spatial resolution of the imagery, or in areas where the occurrence of spectral mixing is low. Soft image classification is the process of deriving the abundance of one or more classes within a single image pixel (Figure 2-3). Soft image classification is useful in areas where the object being classified is finer than the spatial resolution of the image and in areas where the occurrence of spectral mixing is high. Numerous methods have been developed to perform both hard and soft image classification for a range of different sensors and ecosystems (Lu and Weng, 2007; Keshava and Mustard, 2002).

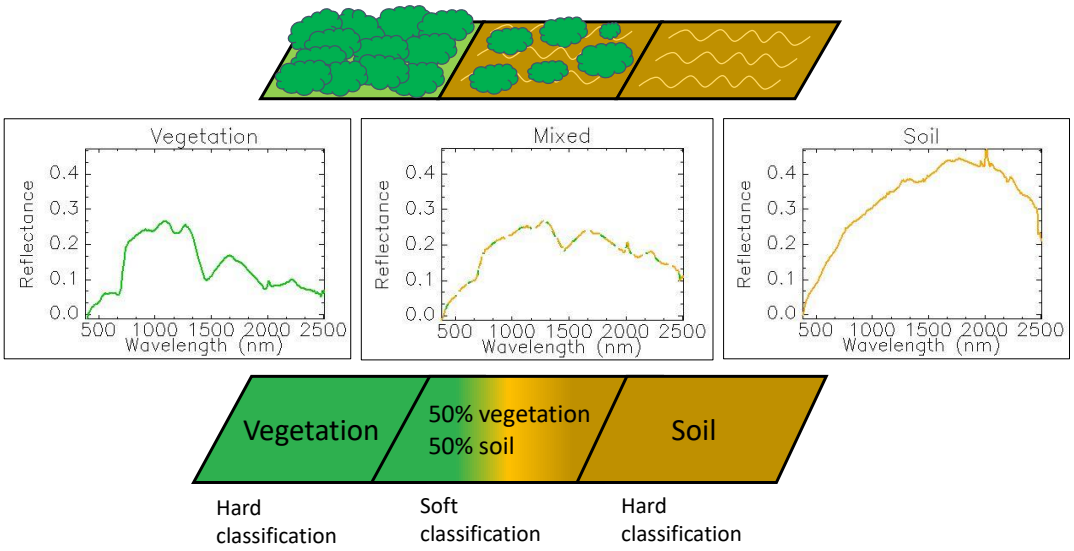

Figure 2-3: Hard classification, depicted on the upper and lower right and left panels (pixels), produces a one class per-pixel output. Soft classification, depicted in the upper and lower middle panels (pixels), produces the abundances of the materials within a pixel. Image spectra are displayed in middle row: pure vegetation (left), pure soil (right), and a mixture of vegetation and soil (middle).

One of the most common hard classification techniques is spectral angle mapper (SAM). SAM treats each spectrum as a vector in space, where the direction of the vector represents the shape of the spectral signature and length represents the recorded reflectance. SAM matches image spectra to EM to find the EM which best represents the

recorded signature, defined as the EM that produces the smallest spectral angle when compared to the image spectrum (Equation 1) (Kruse et al., 1993). SAM has been effective in classifying and distinguishing between deciduous and evergreen vegetation in semi-arid ecosystems in past studies (Yang et al., 2009; Cho et al., 2010; George et al., 2014).

$$SAM = cos^{-1}\left(\frac{\sum_{i=1}^{b} p_i e_i}{\left(\sum_{i=1}^{b} p_i^2\right)^{1/2}\left(\sum_{i=1}^{b} e_i^2\right)^{1/2}}\right)$$

Equation 1: Spectral angle mapper (SAM), where p = pixel spectrum, e = endmember spectrum (EM), i = band number, and b = total number of bands. Pixel membership is assigned to the EM that produces the lowest value when compared to that pixel's spectrum.

Spectral mixture analysis is a soft image classification technique used to estimate the percent of an EM within a given spatial area (Equation 2 and Figure 2-4). This method uses a linear mixing model which assumes a unique EM within a pixel is isolated within an area and the size of this area controls the influence an EM has on the mixed spectrum (Settle and Drake, 1993; Bioucas-Dias et al., 2012). The recorded mixed spectrum is a combination of an EM and an error component, which is a representation of the naturally occurring spectral variations. Roberts et al. (1993) developed a method to alter the number of EM that could contribute to a single spectrum, giving the abundances of multiple materials in a single pixel, coined multiple endmember spectral mixture analysis (MESMA). This method compares each spectrum as a linear combination of different EM and an error term, and selects the model that minimizes the error to represent the mixed spectrum. MESMA allows the number of EM within a pixel can vary

on a per pixel basis, creating a flexible model that can capture complex landscape conditions.

$$S_i = \sum_{k=1}^{N} a_{ki} e_k + \varepsilon_i$$

Equation 2: Linear spectral mixture model. S = mixed spectrum at location i, a = abundance of endmember (EM) k at i, e = EM spectrum, N = total number of EM, and ε = error at i.

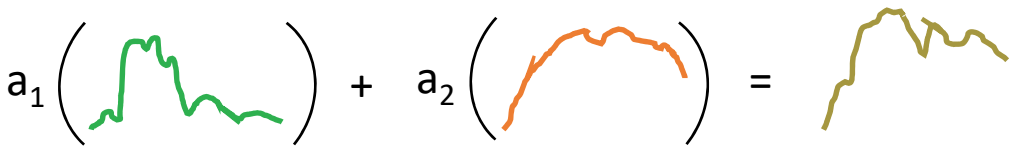

Figure 2-4: Multiple Endmember Spectral Mixture Analysis (MESMA) uses references endmembers (EM) (left) to describe the observed mixed spectral signature (right). Abundances a_1 and a_2 are solved for through an inverse method.

EM for hard and soft image classification can be either derived from a reference spectral library or extracted from an image at locations where pixels are known to be homogeneous. Reference spectra often represent the purest reflectance of an EM without any interference from unwanted components, where image-derived EM represent the reflectance of an EM at a coarser scale, thus containing reflectance from other materials (i.e. library reflectance of a leaf vs. image reflectance of a canopy). Spectral properties of vegetation often vary across an image due to several factors including canopy structure, foliar chemistry, leaf size and orientation, and solar angle (Asner at al., 1998; Ollinger et al., 2002; Asner et al., 2009; Kokaly et al., 2009). Image derived EM are better at capturing this variability because the reflectance values extracted from the image are a function of all these variables (Drake et al, 1999; Bateson et al., 2000; Glenn et al., 2005; Keshava and Mustard, 2002). Bateson et al., 2000, developed a method to further reduce

errors in image classification caused by spectral variability by developing groups, or bundles, of EM all belonging to the same class that would effectively capture the interclass variability observed across an image. These EM bundles are used in place of a single pure EM for a class during hard and soft image classification to increase classification accuracy (Asner and Heidebrecht, 2002; Somers et al., 2011; Zare and Ho, 2014; Dudley et al., 2015; Roth et al., 2015).

In order to determine the effectiveness of an image classification, an accuracy assessment must be performed. Often, a confusion matrix is used for accuracy assessment by using known locations of each of the classes being classified to assess if the classification method accurately predicted these locations. A confusion matrix can also be used to calculate several metrics that determine the effectiveness of the classification method performed, such as overall accuracy, kappa coefficient, and user's and producer's accuracy. Table 2-1 gives an overview of each of these metrics that are used to assess both hard and soft classification accuracies. Commonly reported accuracy assessments for image classification are overall accuracy and kappa coefficient. These two metrics are highly correlated, where overall accuracy is a score of the total accuracy of all the classes classified and the kappa coefficient is a score of the overall accuracy which also accountants for classification that may have occurred by chance. Providing both these metrics is a more robust way to assess the effectiveness of an image classification. Producer's and user's accuracies are metrics that are provided for individual classes and provide information on where under- and over-classification is occurring. Producer's accuracy informs the map producer on how well the classification technique worked and user's accuracy informs the map user on the probability that any given location on the

map is correctly classified. For example, a high producer's accuracy and low user's accuracy for an individual class indicates that an overall over-classification for that class occurred, where a low producer's accuracy and high user's accuracy indicates an overall under-classification occurred for that class.

Table 2-1: Image classification accuracy assessments metrics.

Accuracy assessment metric	Formula	Description
Overall accuracy (OA)	$OA = \frac{Reference\ samples\ correctly\ classified}{Total\ reference\ samples}$	Overall accuracy of classification
Kappa coefficient (K)	$K = \frac{Observed\ accuracy - chance\ agreement}{1 - chance\ agreement}$	Overall accuracy of classification with inclusion of correctly classifying by chance
User's accuracy (UA)	$UA = \frac{Correctly\ classified\ pixels\ in\ a\ class}{Total\ pixels\ classified\ in\ a\ class}$	How accurate is the map for a given class?
Producer's accuracy (PA)	$PA = \frac{Reference\ pixels\ correctly\ classified}{Total\ reference\ pixels\ in\ a\ class}$	How well did the classification method work?

References

Asner, G. P., & Heidebrecht, K. B. (2002). Spectral unmixing of vegetation, soil and dry carbon cover in arid regions: Comparing multispectral and hyperspectral observations. *International Journal of Remote Sensing, 23*(19), 3939-3958. doi:10.1080/01431160110115960

Asner, G. P., Bateson, C. A., Privette, J. L., Saleous, N. E., & Wessman, C. A. (1998). Estimating vegetation structural effects on carbon uptake using satellite data fusion and inverse modeling. *Journal of Geophysical Research: Atmospheres, 103*(D22), 28839-28853. doi:10.1029/98jd02459

Asner, G. P., Martin, R. E., Ford, A. J., Metcalfe, D. J., & Liddell, M. J. (2009). Leaf chemical and spectral diversity in Australian tropical forests. *Ecological Applications, 19*(1), 236-253. doi:10.1890/08-0023.1

Ballanti, L., Blesius, L., Hines, E., & Kruse, B. (2016). Tree Species Classification Using Hyperspectral Imagery: A Comparison of Two Classifiers. *Remote Sensing, 8*(6), 445. doi:10.3390/rs8060445

Bateson, C., Asner, G., & Wessman, C. (2000). Endmember bundles: a new approach to incorporating endmember variability into spectral mixture analysis. *IEEE Transactions on Geoscience and Remote Sensing, 38*(2), 1083-1094. doi:10.1109/36.841987

Bioucas-Dias, J. M., Plaza, A., Dobigeon, N., Parente, M., Du, Q., Gader, P., & Chanussot, J. (2012). Hyperspectral Unmixing Overview: Geometrical, Statistical, and Sparse Regression-Based Approaches. *IEEE Journal of Selected Topics in Applied Earth Observations and Remote Sensing, 5*(2), 354-379. doi:10.1109/jstars.2012.2194696

Campbell, J. B., & Wynne, R. H. (2011). *Introduction to remote sensing*. New York: Guilford.

Cho, M. A., Debba, P., Mathieu, R., Naidoo, L., Aardt, J. V., & Asner, G. P. (2010). Improving Discrimination of Savanna Tree Species Through a Multiple-Endmember Spectral Angle Mapper Approach: Canopy-Level Analysis. *IEEE Transactions on Geoscience and Remote Sensing, 48*(11), 4133-4142. doi:10.1109/tgrs.2010.2058579

Drake, N. A., Mackin, S., & Settle, J. J. (1999). Mapping Vegetation, Soils, and Geology in Semiarid Shrublands Using Spectral Matching and Mixture Modeling of SWIR AVIRIS Imagery. *Remote Sensing of Environment, 68*(1), 12-25. doi:10.1016/s0034-4257(98)00097-2

Dudley, K. L., Dennison, P. E., Roth, K. L., Roberts, D. A., & Coates, A. R. (2015). A multi-temporal spectral library approach for mapping vegetation species across spatial and temporal phenological gradients. *Remote Sensing of Environment, 167*, 121-134. doi:10.1016/j.rse.2015.05.004

Eckmann, T. C., Roberts, D. A., & Still, C. J. (2009). Estimating subpixel fire sizes and temperatures from ASTER using multiple endmember spectral mixture analysis. *International Journal of Remote Sensing,30*(22), 5851-5864. doi:10.1080/01431160902748531

George, R., Padalia, H., & Kushwaha, S. (2014). Forest tree species discrimination in western Himalaya using EO-1 Hyperion. *International Journal of Applied Earth Observation and Geoinformation, 28,* 140-149. doi:10.1016/j.jag.2013.11.011

Ghiyamat, A., Shafri, H. Z., Mahdiraji, G. A., Shariff, A. R., & Mansor, S. (2013). Hyperspectral discrimination of tree species with different classifications using single- and multiple-endmember. *International Journal of Applied Earth Observation and Geoinformation, 23,* 177-191. doi:10.1016/j.jag.2013.01.004

Glenn, N. F., Mundt, J. T., Weber, K. T., Prather, T. S., Lass, L. W., & Pettingill, J. (2005). Hyperspectral data processing for repeat detection of small infestations of leafy spurge. *Remote Sensing of Environment,95*(3), 399-412. doi:10.1016/j.rse.2005.01.003

Heylen, R., Parente, M., & Gader, P. (2014). A Review of Nonlinear Hyperspectral Unmixing Methods. *IEEE Journal of Selected Topics in Applied Earth Observations and Remote Sensing,7*(6), 1844-1868. doi:10.1109/jstars.2014.2320576

Keshava, N., & Mustard, J. (2002). Spectral unmixing. *IEEE Signal Processing Magazine, 19*(1), 44-57. doi:10.1109/79.974727

Kokaly, R. F., Asner, G. P., Ollinger, S. V., Martin, M. E., & Wessman, C. A. (2009). Characterizing canopy biochemistry from imaging spectroscopy and its application to ecosystem studies. *Remote Sensing of Environment, 113*, 578-591. doi:10.1016/j.rse.2008.10.018

Kruse, F. A., Lefkoff, A. B., Boardman, J. W., Heidebrecht, K. B., Shapiro, A. T., Barloon, P. J., & Goetz, A. F. H. (1993). The spectral image processing system (SIPS)—interactive visualization and analysis of imaging spectrometer data. *Remote sensing of environment, 44*(2-3), 145-163

Lawrence, R. L., Wood, S. D., & Sheley, R. L. (2006). Mapping invasive plants using hyperspectral imagery and Breiman Cutler classifications (randomForest). *Remote Sensing of Environment, 100*(3), 356-362. doi:10.1016/j.rse.2005.10.014

Lu, D., & Weng, Q. (2007). A survey of image classification methods and techniques for improving classification performance. International Journal of Remote Sensing, 28(5), 823-870. doi:10.1080/01431160600746456

Okin, G. S., Roberts, D. A., Murray, B., & Okin, W. J. (2001). Practical limits on hyperspectral vegetation discrimination in arid and semiarid environments. *Remote Sensing of Environment, 77*(2), 212-225. doi:10.1016/s0034-4257(01)00207-3

Okin, G. S., & Roberts, D. A. (2004). Remote sensing in arid regions: challenges and oppurtunities.

Ollinger, S. V., Smith, M. L., Martin, M. E., Hallett, R. A., Goodale, C. L., & Aber, J. D. (2002). Regional Variation in Foliar Chemistry and N Cycling among Forests of Diverse History and Composition. *Ecology*, *83*(2), 339. doi:10.2307/2680018

Qin, W., & Gerstl, S. A. (2000). 3-D Scene Modeling of Semidesert Vegetation Cover and its Radiation Regime. *Remote Sensing of Environment,74*(1), 145-162. doi:10.1016/s0034-4257(00)00129-2

Roberts, D., Smith, M., & Adams, J. (1993). Green vegetation, nonphotosynthetic vegetation, and soils in AVIRIS data. *Remote Sensing of Environment, 44*(2-3), 255-269. doi:10.1016/0034-4257(93)90020-x

Roth, K. L., Roberts, D. A., Dennison, P. E., Alonzo, M., Peterson, S. H., & Beland, M. (2015). Differentiating plant species within and across diverse ecosystems with imaging spectroscopy. *Remote Sensing of Environment,167*, 135-151. doi:10.1016/j.rse.2015.05.007

Settle, J. J., & Drake, N. A. (1993). Linear mixing and the estimation of ground cover proportions. *International Journal of Remote Sensing,14*(6), 1159-1177. doi:10.1080/01431169308904402

Somers, B., Asner, G. P., Tits, L., & Coppin, P. (2011). Endmember variability in Spectral Mixture Analysis: A review. *Remote Sensing of Environment, 115*(7), 1603-1616. doi:10.1016/j.rse.2011.03.003

Underwood, E. (2003). Mapping nonnative plants using hyperspectral imagery. *Remote Sensing of Environment,86*(2), 150-161. doi:10.1016/s0034-4257(03)00096-8

Zare, A., & Ho, K. (2014). Endmember Variability in Hyperspectral Analysis: Addressing Spectral Variability During Spectral Unmixing. *IEEE Signal Processing Magazine, 31*(1), 95-104. doi:10.1109/msp.2013.2279177

CHAPTER THREE: HYPERSPECTRAL DERIVED VEGETATION SPECIES AND COVER ACROSS LANDSCAPE GRADIENTS IN A SEMI-ARID ECOSYSTEM USING MULTIPLE ENDMEMBER SPECTRAL MIXTURE ANALYSIS COUPLED WITH OPTIMAL ENDMEMBER BUNDLING

1. Introduction

The ability to determine vegetation species and cover across ecotones in semi-arid regions with large environmental gradients provides a reference state to track changes in the vegetation communities over time. Tracking these changes allow scientists and land managers to understand the vulnerability and flux of vegetation in semi-arid ecosystems caused by the increase in frequency of wildfires (Balch et al., 2012), droughts (Yi et al., 2015), and the spread of invasive species (Chambers et al., 2007). Moreover, the change in vegetation composition caused by these environmental disturbances is correlated to the total carbon within the landscape (Miller et al., 2011); where the loss of the ecosystem's native vegetation can lead to a decrease in carbon storage (Reichstein et al., 2013). This loss of carbon storage is vital at the global scale, where semi-arid ecosystems have a large impact on the interannual global carbon variability (Poulter et al., 2014). Mapping the current distribution of species within the different biomes of semi-arid ecosystems will improve current carbon estimates and provide information to better quantify the effects vegetation has on global carbon levels and climate change (Reichstein et al., 2013; Thomey et al., 2014; Scott et al., 2015).

Image spectroscopy (hyperspectral imagery) has been used to classify species of vegetation within a range of different biomes (e.g. Asner and Heidebrecht, 2002; Adam et al., 2010; George et al., 2014; Roth et al., 2015; Ballanti et al., 2016). The large environmental gradients (i.e. elevation) and variability in climate in mountainous semi-arid ecosystems creates the necessary conditions for multiple biomes to exist within close proximity to each other (Reid, 2005; Dufour et al., 2006; Hofer et al., 2008). Wetter, higher elevation and riparian areas are populated with alpine and deciduous vegetation, respectively, while drier, lower elevation portions of the landscape are dominated by shrubland vegetation. There are many challenges associated with classifying vegetation species across these regions, as the physical properties of each vegetation community contributes a unique remote sensing phenomena. For example, in semi-arid regions there exist both densely populated regions with complex species interactions that are characterized by a high spectral variability and regions populated with sparse vegetation masked by soil albedo (Hall et al., 2008; Adam et al., 2010; Okin and Roberts, 2004).

Hyperspectral imagery has been used in the past to overcome the challenges presented by remote sensing the unique physical properties of different vegetation communities. George et al. (2014) used hyperspectral imagery to classify vegetation species in mountainous regions. Madritch et al. (2014) incorporated multiple spectral properties of different aged aspen stands to account for the spectral variability observed between the stands. Other studies have used linear spectral unmixing models to estimates shrub abundance in sagebrush steppe ecosystems (Okin and Roberts, 2004; Thorp et al., 2013; Roth et al., 2015). Most previous studies focused on classifying landscape scale vegetation have relied on medium to coarse spatial resolution imagery that often mask

any ecotones present (Thorp et al., 2013; George et al., 2014; Mitchell et al., 2015; Roth et al., 2015). The high spatial resolution (1 m) hyperspectral imagery necessary to classify biomes with high spectral diversity and strong spectral mixing, and capture the ecotones between them is rarely available at the landscape scale.

The aim of this study is to develop and assess the capability to derive vegetation species and cover across ecotones and environmental gradients in a semi-arid ecosystem at a high spatial resolution (1 m). We hypothesize hyperspectral imagery, coupled with multiple endmember classification techniques, can accurately classify vegetation with contrasting spectral characteristics caused by the occurrence of ecotones and large environmental gradients present in semi-arid regions.

Background

Spectral angle mapper (SAM) is a common image classification technique that has been used in conjunction with hyperspectral imagery to classify evergreen and deciduous forest (Cho et al., 2010), detect juniper expansion (Yang et al., 2009), and classify vegetation over hilly terrain (George et al., 2014). SAM compares image spectra with reference spectra, or endmembers (EM), by mapping each spectrum as a vector in a n-dimensional space and measuring the angle between the two vectors. SAM only compares the direction of the two vectors and is invariant to changes in spectral intensity between spectra with similar shapes (Ghiyamat et al., 2013). It has been noted that because of this, SAM is an effective method in classifying areas with variations in spectral albedo such as riparian zones, mixed forest, and dense canopies (Shrestha et al., 2002; Dennison et al., 2004; Hestir et al., 2008).

Although SAM has been effective at classifying vegetation in areas where spectral signatures are well defined (i.e. tree canopies), it has limitations in areas of high spectral mixing (Shrestha et al., 2002; Dennison et al., 2004). Spectral mixing often occurs in heterogeneous areas where vegetation cover is low and image spectra are composed of multiple unique EM. Abundances of EM within a mixed spectrum can be derived through an inverse problem using a linear mixture model (LMM) (Bioucas-Dias et al., 2012). LMM have been shown to be sufficient at approximating vegetation cover from areas of high spectral mixing (Qin and Gerstl, 2000; Keshava and Mustard, 2002; Bioucas-Dias et al., 2012). By detecting the partial contribution of an EM within a mixed signal, LMM is able to determine vegetation abundance in low cover areas where soil exposure is high (e.g. sagebrush steppe).

Often estimating the abundance of a single EM within a pixel is not sufficient to represent the heterogeneous landscapes of semi-arid ecosystems. Multiple endmember spectral mixture analysis (MESMA) is a LMM developed by Roberts et al., 1998 as an approach to deal with these complex systems by incorporating the option of multiple EM contributing to mixed spectra. MESMA has shown potential in estimating vegetation in shrubland biomes where sparse vegetation and the large exposure of soil often contribute to the occurrence of widespread spectral mixing (Okin et al., 2001; Asner and Heidebrecht, 2002; Thorp et al., 2013; Roth et al., 2015). Unlike SAM, MESMA is extremely sensitive to changes in spectral albedo of an EM because it assumes each EM is a pure representation of a given class. This causes the need of many EM to represent areas where the structure of an object's spectrum is fixed but the spectral intensity varies,

such as dense tree canopies (Dennison et al., 2004; Fan and Deng, 2014; Roth et al., 2015).

A standardized method to assess the accuracy of sub-pixel estimates produced by spectral unmixing techniques such as MESMA has not yet been established in the literature (Foody et al., 2005; Sliván-Cárdenas and Wang, 2008). Past studies have relied on techniques such as the use of fine spatial-scale imagery, vegetation indices, and statistical metrics (e.g. RMSE) to gauge the estimates produced from spectral unmixing (Thorp et al., 2013; Fan and Deng, 2014; Roth et al., 2015). Silván-Cárdenas and Wang (2008) developed a specialized confusion matrix that evaluates the performance of linear spectral unmixing techniques, termed sub-pixel confusion-uncertainty matrix (SCM). A SCM calculates the accuracy of sub-pixel estimates with the use of field measured class cover instead of determining if a location was correctly classified or not, as in a traditional confusion matrix. The method uses a composite operator, p_{nij}, to calculate the SCM:

$$p_{nij} = \begin{cases} MIN(c_{ni}, f_{nj}), & i = j \\ (c_{ni} - p_{nii}) \times \left[\dfrac{f_{nj} - p_{njj}}{\sum_{j=1}^{k} (f_{nj} - p_{njj})} \right], & i \neq j \end{cases}$$

Equation 3: Sub-pixel confusion-uncertainty matrix (SCM)

where p is the specific cell in the SCM for pixel n, c is the class cover produced from the LMM for pixel n, f is the field measure class cover for pixel n, MIN is the minimum value between the derived and field cover, k is the total number of classes, and i and j represent the row and column of the SCM, respectively. Since the boundaries of the multiple classes present within a pixel are undefined in both the image and field data, the

SCM cannot determine where misclassification is occurring between classes. Instead, the SCM can be used to calculate standard accuracy metrics such as overall accuracy, kappa coefficient, producer's accuracy (PA), and user's accuracy (UA). SCM is an ideal method to assess spectral unmixing accuracies where there are sufficient field data available (Chen et al., 2010; Frazier and Wang, 2011).

Classification accuracy with both SAM and MESMA are dependent on the optimal selection of EM that best represent the observed reflectance of an object within an image (Cho et al., 2010; Somers et al., 2011; Ghiyamat et al., 2013; Roth et al., 2015). Reflectance is a factor of physical properties such as leaf orientation, leaf chemical composition, canopy structure, solar angle, vegetation age, and soil and littler exposure and composition (Asner et al., 1998; Ollinger et al., 2002; Asner et al., 2009; Kokaly et al., 2009). These factors can cause reflectance from vegetation within the same class to vary across an image (Figure 3-1). The use of image-derived spectra for classification better captures the observed spectral variability when compared to EM derived from field spectrometers or reference libraries (Drake et al, 1999; Bateson et al., 2000; Keshava and Mustard, 2002). Classification accuracy can be further increased by using groups or bundles of EM to capture the inter-class variability caused by the reasons stated above (Bateson et al., 2000; Cho et al., 2010; Zare and Ho, 2014; Dudley et al., 2015). The combination of optimal EM selection and EM bundling can increase the accuracy of vegetation classification using both SAM and MESMA.

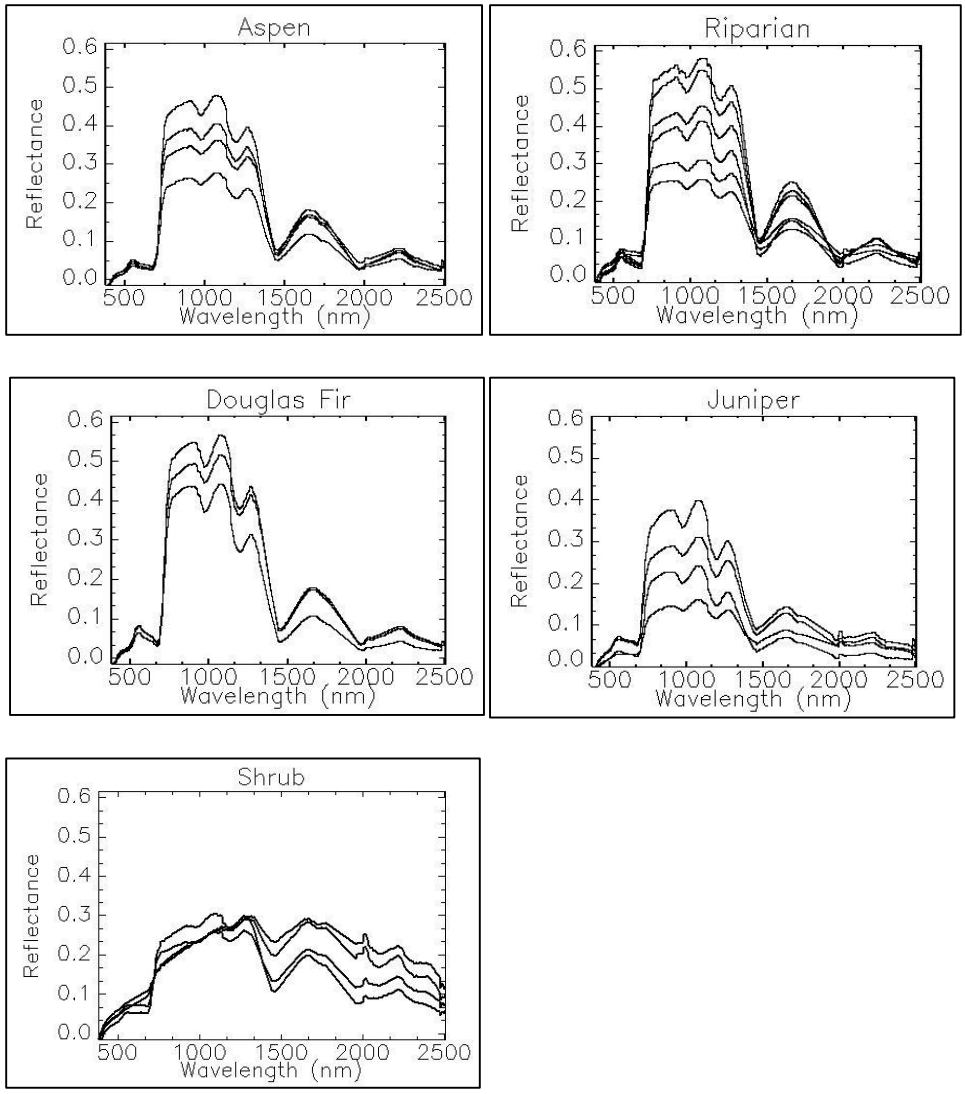

Figure 3-1: Spectral variation within each vegetation class extracted from multiple portions of the image and across RCEW. Aspen (top left), Riparian (top right), Douglas Fir (middle left), Juniper (middle right), and Shrub (bottom left).

Methods

Study Area

This study was conducted in Reynolds Creek Experimental Watershed (RCEW), located in the Owyhee Mountains, ID (Figure 3-2). RCEW encompasses 23,900 ha of semi-arid ecosystem and has an elevation gradient of ranging from 900-2100 m (Seyfried et al., 2000). Annual mean precipitation ranges from 250-1100 mm in a linear trend with

elevation (Marks et al., 2007). RCEW can be divided into three major biomes defined by both sharp and gradual ecotones. Alpine vegetation dominates higher elevations in the southern portion of the watershed and consists primarily of quaking aspen (*Populus termuloides*), Douglas fir (*Psuedotsuga menziesii*), and western juniper (*Juniperus occidentalis*) (Seyfried et al., 2000). There is a gradual transition into the lower elevations in the northern portion of the watershed consisting primarily of Wyoming big sagebrush (*Artemisia tridentate* ssp. *wyomingensis*), low sagebrush (*Artemisia arbuscula*), rabbitbrush (*Ericameria nauseosa*) and bitterbrush (*Pushia tridentate*). This ecotone contains western juniper that is expanding downward in elevation into the lower elevation shrub communities. Several grass communities consisting of bluebunch wheatgrass (*Pseudoroegneria spicata*), needle and thread (*Hesperostipa comata*), western wheatgrass (*Pascopyrum smithii*), tapertip hawksbeard (*Crepis acuminata*), and yarrow (*Achillea millefolium*) also populate these areas (Pyke et al., 2015). The final biome within RCEW is defined as the riparian areas of the watershed. Common riparian vegetation in the region are black cottonwood (Populus *trichocarpa*), coyote willow (*Salix exigua*), and peachleaf willow (*Salix amygdaloides*) (National Research Council, 2002). Riparian regions transition gradually into alpine vegetation in the higher elevation areas; whereas the transition between riparian regions and shrublands is much sharper in the lower elevations.

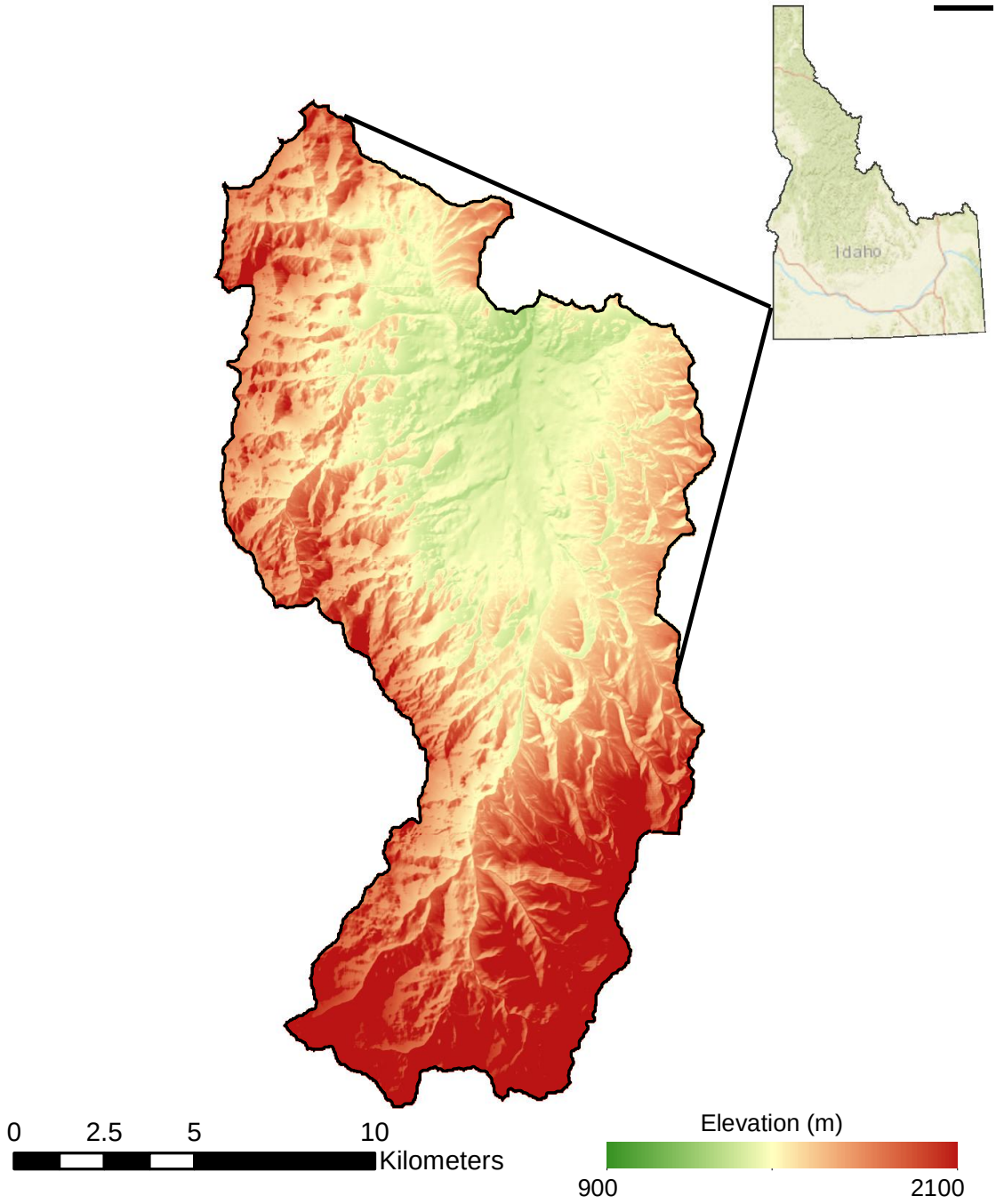

Figure 3-2: Reynolds Creek Experimental Watershed (RCEW) location. Elevation displayed at a 1 m scale.

Data

Field data and imagery were collected in 2014-2016 as part of a NASA Terrestrial Ecology (TE) project campaign (NASA Terrestrial Ecology NNX14AD81G). The objective of this study was to quantify vegetation characteristics in semi-arid ecosystems using remote sensing techniques, such as hyperspectral and full waveform lidar (NNX14AD81G; PIs: Glenn, Ustin, Mitchell, Flores). Locations for areas where each tree species (aspen, Douglas fir, juniper, and riparian) was the dominate cover were collected across the watershed using a Topcon HiPer V Real Time Kinematic (RTK) GPS. Shrub, grass and soil cover was measured at 48 plots (10*10 m) across RCEW for a range of elevation, cover, and species. A list of plot locations and characteristics is located in Appendix A. Sample Point photo analysis (Booth et al., 2006) was used to classify each plot using a series of 20 photos taken every 2 m across the plot. Dominant vegetation cover for the collected plots included: sagebrush, bitterbrush, rabbitbrush, mixed shrub, and grasses.

Hyperspectral imagery were collected on June 11th 2015 using NASA's Airborne Visible and Infrared Imaging Spectrometer Next Generation (AVIRIS-ng) sensor over 380-2500 nm using 432 spectral bands with a bandwidth of about 5 nm. NASA's AVIRIS-ng level two product, consisting of orthorectified surface reflectance atmospherically corrected with ATREM (Gao et al., 2009), was used for this study. A total of 15 AVIRIS-ng images were used to capture the full extent of RCEW. While maintaining a consistent spatial resolution during the data collection, approximately 17 km^2 (~6%) of the total watershed was not captured, resulting in several gaps between the images. The original pixel size of 1.5 m for each image was resampled down to 1 m using

a bilinear interpolation when the image was georegistered to 1 m lidar imagery. The error of this registration is about half a pixel or 0.5 m. Spectral bands were inspected for noise caused from atmospheric water absorption, and 59 of the original bands were removed.

Endmember Derivation

Individual 1 m pixels were delineated from the AVIRIS-ng imagery using a combination of field data from the NASA TE campaign and additional independent field locations for all species considered for this study: aspen, riparian, Douglas fir, juniper, shrubs (sagebrush, bitterbrush, and rabbitbrush), and grasses. Approximately 20% of the total field data for each class was randomly selected as training data for the classification, with the additional 80% used for validation. EM bundles were built from the extracted image spectra for each of the listed classes, and used to capture the spectral variability observed over the image.

Open-source software Visualization and Image Processing for Environmental Research (VIPER, Version 2.0) was used to compile and build EM bundles from the extracted image spectra for each class to be used during the classification process. The VIPER toolbox calculates several statistical metrics including endmember average root mean square error (EAR) and minimum average spectral angle (MASA) to highlight inter-class spectrally variability and ultimately choose spectral bundles that best represent an entire class. EAR is the average RMSE produced by an EM when it is used to model all other EM of the same class, where the lowest EAR is a measure of which spectra can best represent that class. MASA, similar to EAR, uses each EM to model all other EM of the same class, but compares the spectral angle produced between the two spectra to find the EM that produces the lowest error.

Spectral libraries were reduced to a smaller subset from the original extracted spectra through an iterative process of taking the top spectra with the highest EAR and MASA results, running the classification process on several random validation plots, and removing spectra that performed poorly or were unused. This process was repeated until removing spectra decreased classification results. This procedure helped reduce computation time and the number of training samples used, and it maximized the number of validation samples. Table 3-1 shows the number of spectra per class that were delineated in the initial spectral library, the number of samples used in the final classification, and the number of samples used for classification validation. Field plots that did not have spectra used in the final spectral libraries were used to assess the classification accuracy.

Table 3-1: The number of ground validation points (represented by 1 m pixels) used for endmember (EM) derivation and classification accuracy assessment per class.

Class	Image extracted EM	EM used in final classification	Validation samples	Classification method
Aspen	1004	3	4816	SAM
Riparian	1316	5	3271	SAM
Douglas Fir	90	3	3947	SAM
Juniper	187	3	1409	SAM
Sagebrush	141	5	2600	MESMA
Bitterbrush	82	2	800	MESMA
Grass	46	2	3400	MESMA
Soil	100	3	3400	MESMA

Classification

Classification was performed using all the AVIRIS-ng bands after pre-processing (n=373) over the collected spectrum (380-2500 nm) with a combination of SAM and MESMA. SAM was used to classify tree vegetation within RCEW located in the riparian zones and higher elevations of the watershed in order to account the high spectral

diversity of these areas. A shrubland class, comprised of a mixture of shrubs, grass, litter, and soil, was incorporated for classification, and validation data, along with visual inspections, were used to ensure these areas were appropriately labeled. The maximum allowable spectral angle for SAM was set to 0.1 radians. A post classification 3x3-pixel moving average filter was performed in ENVI to enhance spatial consistency of the SAM results. SAM classification of aspen, riparian, Douglas fir, and juniper were masked out of the imagery before MESMA computation for the remaining classes.

MESMA was used to derive abundances of shrubs, grasses, and soil within the watershed where spectral mixing is occurring due to the small structure and low cover of these vegetation classes. The MESMA parameters of minimum and maximum allowable EM fraction, minimum and maximum allowable shade fraction, and maximum allowable RMSE were set 0.0, 1.0, 0.0, 0.8 and 0.025, respectively. These values were set based on performance from trial and error. Model complexity, defined by the allowable number of EMs per pixel, was set to three; this includes the combination of two class EM from the spectral library and a shade component, which was set to photometric (zero) for this study. A three-EM complexity approach was chosen because when given the option of modeling a pixel with two-EM, MESMA consistently chose this, which did not accurately represent the heterogeneity of the landscape observed in the field. The absence of either a grass or soil EM in the prediction of shrub abundance led to poor results in initial testing. Okin et al. (2001) noted similar results when trying to identify soil composition and abundance in semi-arid ecosystems using MESMA and did not include a vegetation or litter component in their models. A total of 56 models were used during the final unmixing process.

Accuracy Assessment

Accuracy assessment for both classification methods were performed separately using field validation data (Table 3-1). SAM classification was evaluated using standard classification metrics: a confusion matrix, overall accuracy, kappa coefficient, PA, and UA. Because MESMA produces abundances of multiple classes in a single pixel, a traditional confusion matrix cannot be directly applied to assess the accuracy of the cover. In replacement, a SCM was used to assess the accuracy of the abundance derived from MESMA. The SCM was calculated for each plot (10*10 m), then resulting SCM were averaged to produce the final SCM (Chen et al., 2010). An overall accuracy, kappa coefficient, PA, and UA were produced from the final SCM for the shrub, grass, and soil cover.

Results

i. *SAM*

SAM classification accuracy was validated on a species level as listed in Table 3-2. Classification had an overall accuracy of 57.9% and a kappa coefficient of 0.43. Riparian, Douglas fir, and juniper classes showed high classification accuracies of 61.8%, 67.8%, and 78.7%, respectively. The aspen class resulted in low accuracies and significant classification confusion with the riparian class. Therefore classification was recomputed into plant functional types (PFT) with a combined deciduous tree class (aspen and riparian) and combined evergreen tree class (Douglas fir and juniper) (Table 3-3). A PFT classification groups vegetation with similar physical characteristics and are commonly used for ecosystem dynamics and hydrological modeling (Gerten et al., 2004). Overall accuracies for the PFT classification was 84.4% with a kappa coefficient of 0.68.

Deciduous and evergreen classes had accuracies of 88.3% and 77.5%, respectively.

Figure 3-3 shows both the species and PFT vegetation classifications of RCEW.

Table 3-2: Confusion matrix, overall accuracy, kappa coefficient, and user's and producer's accuracies for species classification produced using SAM. The confusion matrix is represented as the number of pixels used for accuracy assessment.

	Ground Truth				
	Aspen	Riparian	Douglas Fir	Juniper	Total
Aspen	**2017**	559	150	0	2726
Riparian	2420	**1838**	364	56	4678
Douglas Fir	106	508	**2195**	112	2921
Juniper	7	0	49	**726**	782
Unclassified	11	69	479	29	588
Total	4561	2974	3237	923	11695

Overall Accuracy = 57.9%		Kappa coefficient = 0.43	
	Class Accuracy	Producer's Accuracy	User's Accuracy
Aspen	44.2%	44%	74%
Riparian	61.8%	62%	39%
Douglas Fir	67.8%	68%	75%
Juniper	78.7%	79%	93%

Table 3-3: Confusion matrix, overall accuracy, kappa coefficient, and user's and producer's accuracies for plant functional type classification produced with SAM. The confusion matrix is represented as the number of pixels used for accuracy assessment.

	Ground Truth		
	Deciduous	Evergreen	Total
Deciduous	**6652**	557	7209
Evergreen	825	**3223**	4048
Unclassified	58	380	438
Total	7535	4160	11695

Overall Accuracy = 84.4%		Kappa coefficient = 0.68	
	Class Accuracy	Producer's Accuracy	User's Accuracy
Deciduous	88.3%	88%	92%
Evergreen	77.5%	77%	80%

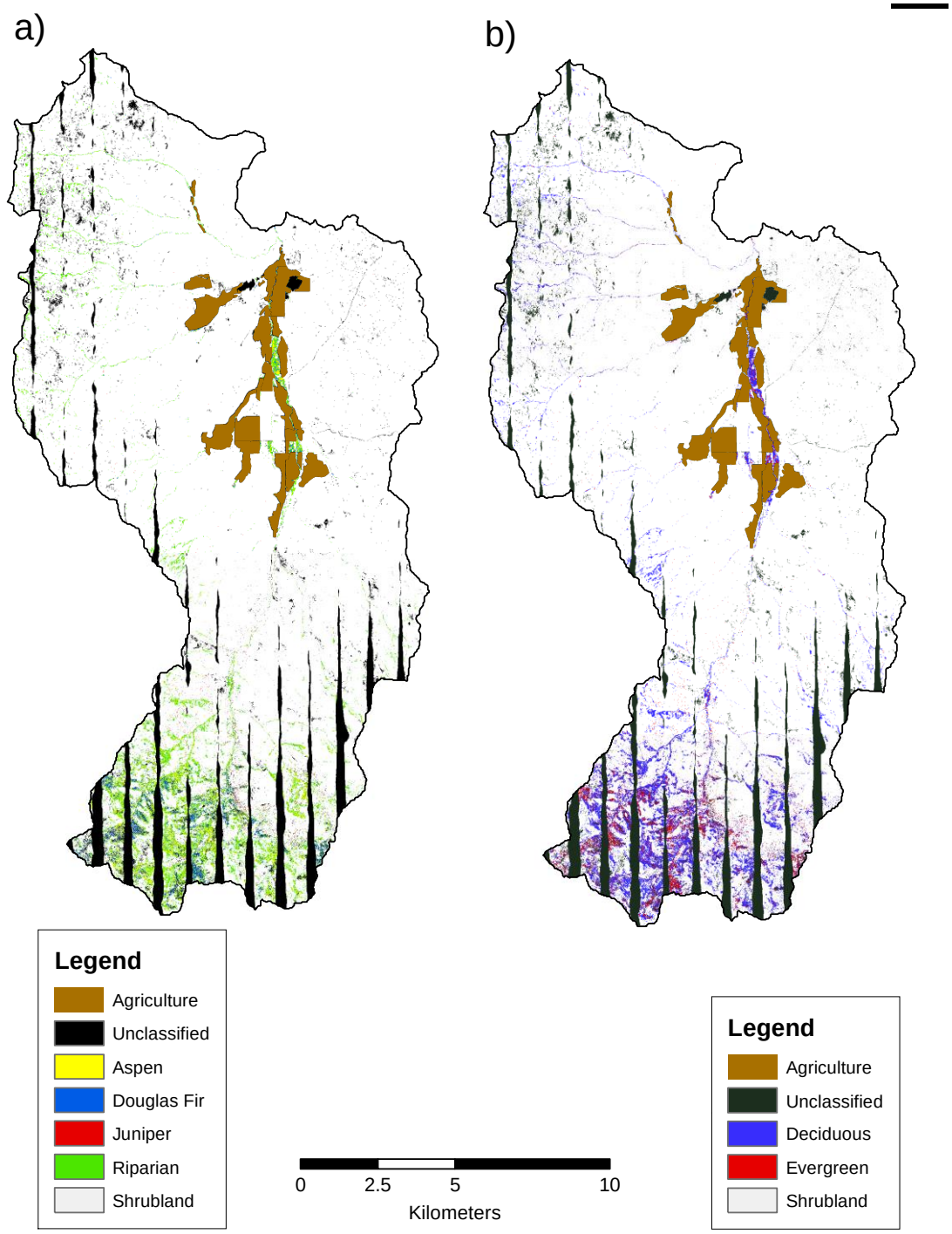

Figure 3-3: Vegetation classification results from SAM in Reynolds Creek Experimental Watershed (RCEW). a) Tree species classification. b) Plant functional types. Note, the black stripes in both classifications are caused from missing data between flightlines and are labeled unclassified.

MESMA

The final SCM for MESMA accuracies was produced using 44 field measured cover (Table 3-4). Overall accuracy derived from the final SCM for the MESMA shrub, grass and soil cover was 67.4%, with a kappa coefficient of 0.53. Both producer's and user's accuracy are listed in Table 3-4. Past studies have stated the inability of remote sensing imagery to predict shrub cover that comprised less than 30% of the landscape (Okin et al., 2001; Thorp et al., 2013). Therefore, the analysis was repeated to observe MESMA estimates in areas where shrub cover was greater than 20% (n= 24 plots). Note, 20% was chosen due to the limited number of field plots in areas that had greater than 30% shrub cover. The SCM for shrub cover >20% is shown in Table 3-5. Results indicate a slight improvement with an overall accuracy of 70.0% and a kappa coefficient of 0.55. Figure 3-4 shows abundancy maps for shrub, grass, and soil classes within RCEW.

Table 3-4: Accuracy metrics derived from the sub-pixel confusion-uncertainty matrix (SCM) to assess abundances derived from MESMA. A total of 44 (10*10 m) plots were used for validation.

Overall Accuracy = 67.4%		Kappa Coefficient = 0.53
	Producer's Accuracy	User's Accuracy
Shrubs	98%	48%
Grass	68%	80%
Soil	48%	93%

Table 3-5: Accuracy metrics derived from the sub-pixel confusion-uncertainty matrix (SCM) to assess abundances derived from MESMA in areas where there was >20% shrub cover present. A total of 24 (10*10 m) plots were used for validation.

Overall Accuracy = 70%		Kappa Coefficient = 0.55
	Producer's Accuracy	User's Accuracy
Shrubs	99%	59%
Grass	79%	76%
Soil	35%	99%

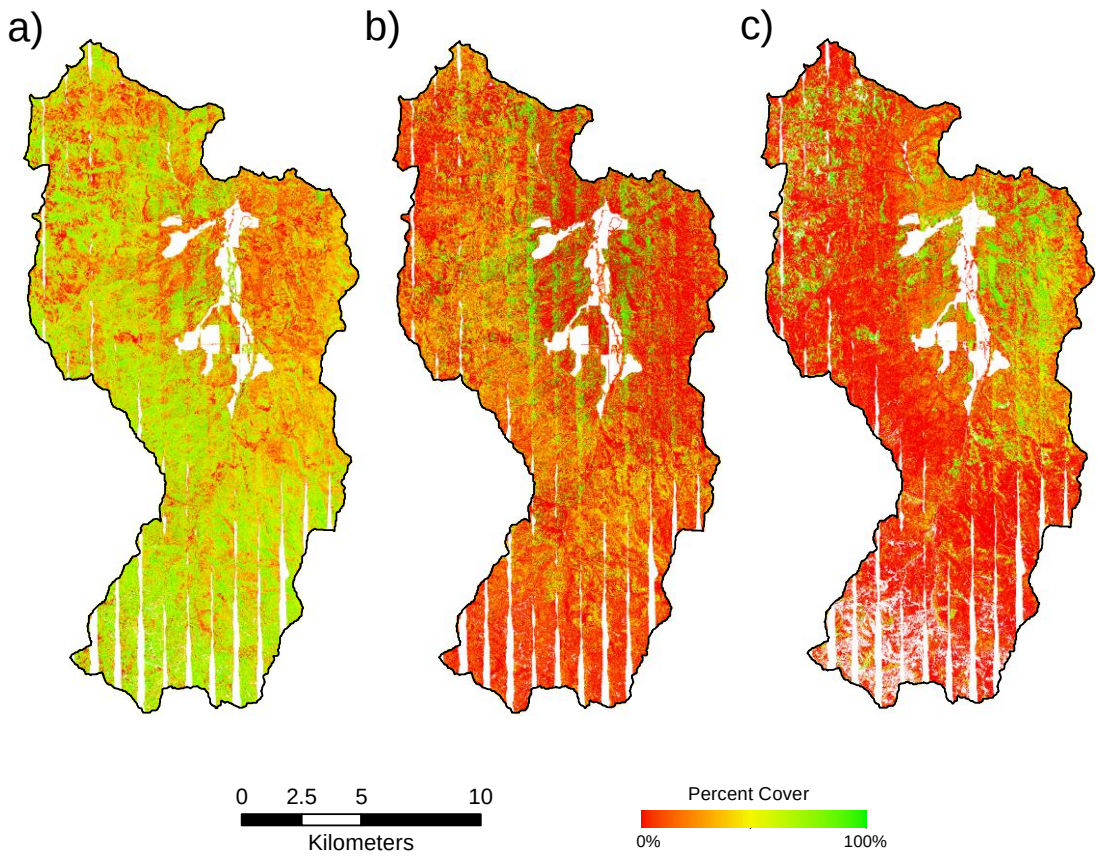

Figure 3-4: Abundancy map produced with multiple endmember spectral mixture analysis (MESMA) for Reynolds Creek Experimental Watershed (RCEW). a) shrub, b) grass, and c) soil. Note, the white stripes are caused from missing data between flightlines.

Discussion

i. Classification of Tree Species and PFT

High spectral and spatial resolution classification of tree species in semi-arid ecosystems is effective but has limitations where there is a complex intergrowth of spectrally similar vegetation species. Past studies classifying deciduous and evergreen species in homogenous ecosystems using SAM had OA ranging from 54%-75% and kappa coefficients of 0.48-0.70 (Cho et al., 2010; George et al., 2014). The main source of classification error in this study was confusion between aspen and riparian areas. Two

factors are believed to contribute to this misclassification, which ultimately lowered the OA and kappa coefficient.

The riparian areas within the study area are characterized by a large diversity of spectral reflectance. Vegetation species present within riparian zones are driven by the surrounding environmental conditions including elevation, precipitation, and soil composition (Patten, 1998; National Research Council, 2002; Richardson et al., 2007). Due to large environmental gradients observed within our study site, it is likely that the composition of vegetation species within riparian areas was also highly varied throughout the study area. Also, several areas along the riparian zones were found to have aspen stands growing mixed within the riparian vegetation during field observations. The presence of such a diverse composition of vegetation species will increase the spectral variability within the riparian zones (Adam et al., 2010; Rocchini et al., 2011).

There was a large variation of reflectance between different aspen stands within the imagery. Past studies have noted that a variation in spectra between aspen stands of different ages is caused by variation in foliar chemistry (Madritch et al., 2014). This variation in aspen reflectance covered much of the same range in reflectance that was noted in the riparian spectra. The intermixture of aspen coupled with the high diversity of spectral reflectance within the aspen class resulted in too much spectral noise to accurately distinguish aspen stands in the study site.

Douglas fir and juniper showed higher classification accuracies, likely since both species had distinguishable spectral signatures from each other and other broad leaf classes within the study area. These two evergreen species are structurally unique from each other, which furthers the ability to better classify them when compared to other

structurally similar deciduous trees. The detection of juniper is important in semi-arid ecosystems because there has been an increase in juniper expansion in shrubland areas, changing the fundamental vegetation composition of the area (Miller and Heyerdahl, 2008). Providing an accurate estimate of where current juniper trees are located provides a baseline for studies investigating the phase of and changes in expansion over time.

Classification accuracy improved after combining species into broader PFT classes. This increase in accuracy is attributed to the PFT's ability to account for the spectral variations caused by the different physical properties between species observed across the landscape. Classification with PFT gives an insight into the spatial distribution of different ecosystem functions, which have important implications in ecosystem modeling (Bonan et al., 2002), vegetation monitoring (Pan et al., 2015), and carbon studies (Wu et al., 2016) in semi-arid ecosystems.

Past studies have shown that the incorporation of structural information from lidar (Mitchell et al., 2015; Wang and Glennie, 2015; Glenn et al., 2016) and phenological information from an image time-series analysis (Dennison and Roberts, 2003; Guo et al., 2003; Dudley et al., 2015) improves species classification accuracy. Although hyperspectral imagery can accurately classify species at the landscape scale, using only spectral information can become problematic in heterogeneous landscapes, especially when using image extracted EM from areas of mixed species. Finding pure pixels to use as EM within these heterogeneous regions can be challenging when accurate and extensive field data are not collected. The incorporation of auxiliary information, such as height, density, and phenological information, combined with the spectral data can lead to better species classification in semi-arid ecosystems.

Abundancy Estimates of Shrub, Grass, and Soil

Shrub, grass, and soil cover predicted with MESMA resulted in accurate estimates. This supports the idea that high spatial (1 m) hyperspectral imagery can provide detailed estimates of shrubland vegetation at the landscape scale. Results improved slightly when including only areas with shrub cover >20%. This corroborates with previous studies that state low shrub cover in a landscape may not be measurable as they are easily masked by the reflectance of the surrounding soil and grasses (Okin et al., 2001; Okin and Roberts, 2004). However, the high spatial AVIRIS-ng imagery accurately derived estimates for all cover that were present within the landscape.

The largest discrepancy within the cover results was observed between the PA and UA of the shrub cover. The high PA and corresponding low UA indicates an overall over-classification of shrub cover within the study area. Although the SCM does not convey where misclassification occurs between classes like a traditional confusion matrix, the corresponding PA and UA derived from the SCM indicated that shrub and soil classes had the largest changes between the two accuracies. A high PA and low UA, and low PA and high UA for the shrub and soil classes, respectively, along with grass PA and UA staying relatively consistent, indicates there was confusion between the shrub and soil classes.

This discovery is somewhat surprising, as pure spectra of shrubs and soil are fundamentally different. This likely indicates there was an EM derived from the image that was used during the MESMA process that was not a “pure” representation of a single class (i.e. a mixed EM of shrub and soil was chosen which then overclassified shrubs). Another likely explanation for this phenomenon could be that the exposure of pure soil

within the watershed is not common, as most of the bare ground contains some portion of litter or woody debris. The spectral reflectance from this material could have easily created spectral confusion between the two classes during the MESMA unmixing. Although shrub cover was over-estimated, abundances derived with AVIRIS-ng imagery still provide more detail than estimates made using traditional multispectral sensors and are sufficient when extracting vegetation information at the landscape scale.

Additional distinction between sagebrush, bitterbrush, and rabbitbrush was also attempted during this study, but results were poor due to the spectral similarities and a limited number of field plots for bitterbrush and rabbitbrush dominated areas. Future research should have a sufficient abundance of field data for individual shrub species to establish unique EM for each species. Predicting shrub cover for all dominate species (sagebrush, bitterbrush, and rabbitbrush) as a single class was successful and the results can be used for monitoring fragmentation of shrub communities (Bukowski and Baker, 2013), aboveground biomass estimation (Eisfelder et al., 2012), and habitat restoration (Pyke et al., 2015). The addition of structural and height lidar information in future studies could help distinguish between shrub species (sagebrush and bitterbrush), as bitterbrush is often denser and taller than sagebrush. These structural differences are not observable in the spectral response recorded during imaging spectroscopy.

Spectral Variability

The large number of AVIRIS-ng images used during this study is noteworthy. The 15 airborne images were collected over approximately two and a half hours to capture the full extent of the study area. It is likely that large changes in sun angles and illumination occurred during this timeframe. Hall et al. (2008) reported changes in

canopy reflectance due to solar illumination occurs during the sub-hourly scale, meaning variations in vegetation reflectance during the AVIRIS-ng collection were inevitable. Additionally, illumination of vegetation was affected by shading caused by topographic features and surrounding vegetation. These shading factors would have also varied in intensity throughout the duration of the image collection. These factors likely influenced the effectiveness of the EM bundles, as EM selected in one image may not have been fully representative of the same vegetation species in a different image of the watershed. These issues are unavoidable when analyzing hyperspectral imagery at the landscape scale. However, EM extraction from multiple images for a single class should be sufficient to capture the spectral variability present.

Conclusion

We found that high spatial resolution hyperspectral imagery has the capacity to accurately classify vegetation across the environmental gradients and ecotones observed in RCEW. The use of high spatial resolution hyperspectral imagery improves vegetation estimates and provides detailed insight into the distribution and boundaries of ecotones within the ecosystem that are not obtainable with spaceborne multispectral imagery. The separation of ecotones showed high success because each biome has unique spectral properties that were highlighted in the imagery. Detecting these ecotones is an important step in monitoring global vegetation change in semi-arid ecosystems that occur across portions of the world including the western United States, southern Australia, central Asia, and South Africa.

Individual species classification within each of the semi-arid biomes was more challenging. Each biome showed high spectral variability both within and between vegetation classes. If extensive and accurate field data are not collected, this variability can be difficult to capture when using image derived endmembers for classification. The selection of appropriate endmembers used to represent each vegetation class dictates the overall accuracy of the classification. Previous studies classifying individual species focused on smaller portions of the landscape (Mollot et al., 2007; Cho et al., 2010; Ballanti et al., 2016). By moving to a landscape-scale vegetation classification, a sacrifice is made to the scale at which species can be represented, as collecting extensive field data on all species present within each biome is both time-consuming and expensive.

The upcoming launch of NASA's spaceborne Hyperspectral Infrared Imager (HyspIRI) will be the first readily available global hyperspectral imager and will provide data to continuously monitor vegetation across landscape gradients and ecotones. HyspIRI will have a coarser spatial resolution (60 m) but will have repeat scans of an area with a temporal resolution of 19 days. The multi-temporal hyperspectral HyspIRI imagery will provide additional phenological information that could be used to distinguish between different deciduous species. Previous studies have found the potential use HyspIRI imagery to estimate shrub cover (Mitchell et al., 2015), discriminate rangeland grasses (Sibanda et al., 2016), and classify vegetation across biomes (Lee et al., 2015). As we move towards using this coarser spatial resolution (60 m) hyperspectral imagery to classify vegetation, the use of spectral unmixing techniques will be necessary to accurately estimating vegetation abundances in semi-arid ecosystems, as the occurrence of spectral mixing at this scale will be unavoidable.

Even at these coarser spatial resolutions, these hyperspectral data will provide us with improved estimates of semi-arid vegetation that cannot be resolved with current spaceborne multispectral sensors. Understanding the challenges and limitations associated with vegetation classification using hyperspectral imagery across large environmental gradients and ecotones in semi-arid ecosystems is vital to improve future vegetation estimates and monitor global carbon trends.

References

Adam, E., Mutanga, O., & Rugege, D. (2010). Multispectral and hyperspectral remote sensing for identification and mapping of wetland vegetation: a review. *Wetlands Ecology and Management, 18*(3), 281-296. doi:10.1007/s11273-009-9169-z

Asner, G. P., & Heidebrecht, K. B. (2002). Spectral unmixing of vegetation, soil and dry carbon cover in arid regions: Comparing multispectral and hyperspectral observations. *International Journal of Remote Sensing, 23*(19), 3939-3958. doi:10.1080/01431160110115960

Asner, G. P., Bateson, C. A., Privette, J. L., Saleous, N. E., & Wessman, C. A. (1998). Estimating vegetation structural effects on carbon uptake using satellite data fusion and inverse modeling. *Journal of Geophysical Research: Atmospheres, 103*(D22), 28839-28853. doi:10.1029/98jd02459

Asner, G. P., Martin, R. E., Ford, A. J., Metcalfe, D. J., & Liddell, M. J. (2009). Leaf chemical and spectral diversity in Australian tropical forests. *Ecological Applications, 19*(1), 236-253. doi:10.1890/08-0023.1

Balch, J. K., Bradley, B. A., Dantonio, C. M., & Gómez-Dans, J. (2012). Introduced annual grass increases regional fire activity across the arid western USA (1980-2009). *Global Change Biology, 19*(1), 173-183. doi:10.1111/gcb.12046

Ballanti, L., Blesius, L., Hines, E., & Kruse, B. (2016). Tree Species Classification Using Hyperspectral Imagery: A Comparison of Two Classifiers. *Remote Sensing, 8*(6), 445. doi:10.3390/rs8060445

Bateson, C., Asner, G., & Wessman, C. (2000). Endmember bundles: a new approach to incorporating endmember variability into spectral mixture analysis. *IEEE Transactions on Geoscience and Remote Sensing, 38*(2), 1083-1094. doi:10.1109/36.841987

Bioucas-Dias, J. M., Plaza, A., Dobigeon, N., Parente, M., Du, Q., Gader, P., & Chanussot, J. (2012). Hyperspectral Unmixing Overview: Geometrical, Statistical, and Sparse Regression-Based Approaches. *IEEE Journal of Selected Topics in Applied Earth Observations and Remote Sensing, 5*(2), 354-379. doi:10.1109/jstars.2012.2194696

Bonan, G. B., Levis, S., Kergoat, L., & Oleson, K. W. (2002). Landscapes as patches of plant functional types: An integrating concept for climate and ecosystem models. *Global Biogeochemical Cycles, 16*(2). doi:10.1029/2000gb001360

Booth, D. T., Cox, S. E., & Berryman, R. D. (2006). Point Sampling Digital Imagery with 'Samplepoint'. *Environmental Monitoring and Assessment,123*(1-3), 97-108. doi:10.1007/s10661-005-9164-7

Bukowski, B. E., & Baker, W. L. (2013). Historical fire regimes, reconstructed from land-survey data, led to complexity and fluctuation in sagebrush landscapes. *Ecological Applications, 23*(3), 546-564. doi:10.1890/12-0844.1

Chambers, J. C., Roundy, B. A., Blank, R. R., Meyer, S. E., & Whittaker, A. (2007). What Makes Great Basin Sagebrush Ecosystems Invasible Bybromus Tectorum? *Ecological Monographs, 77*(1), 117-145. doi:10.1890/05-1991

Chen, J., Zhu, X., Imura, H., & Chen, X. (2010). Consistency of accuracy assessment indices for soft classification: Simulation analysis. *ISPRS Journal of Photogrammetry and Remote Sensing, 65*(2), 156-164. doi:10.1016/j.isprsjprs.2009.10.003

Cho, M. A., Debba, P., Mathieu, R., Naidoo, L., Aardt, J. V., & Asner, G. P. (2010). Improving Discrimination of Savanna Tree Species Through a Multiple-Endmember Spectral Angle Mapper Approach: Canopy-Level Analysis. *IEEE*

Transactions on Geoscience and Remote Sensing, 48(11), 4133-4142. doi:10.1109/tgrs.2010.2058579

Dennison, P. E., & Roberts, D. A. (2003). The effects of vegetation phenology on endmember selection and species mapping in southern California chaparral. *Remote Sensing of Environment, 87*(2-3), 295-309. doi:10.1016/j.rse.2003.07.001

Dennison, P. E., Halligan, K. Q., & Roberts, D. A. (2004). A comparison of error metrics and constraints for multiple endmember spectral mixture analysis and spectral angle mapper. *Remote Sensing of Environment, 93*(3), 359-367. doi:10.1016/j.rse.2004.07.013

Drake, N. A., Mackin, S., & Settle, J. J. (1999). Mapping Vegetation, Soils, and Geology in Semiarid Shrublands Using Spectral Matching and Mixture Modeling of SWIR AVIRIS Imagery. *Remote Sensing of Environment, 68*(1), 12-25. doi:10.1016/s0034-4257(98)00097-2

Dudley, K. L., Dennison, P. E., Roth, K. L., Roberts, D. A., & Coates, A. R. (2015). A multi-temporal spectral library approach for mapping vegetation species across spatial and temporal phenological gradients. *Remote Sensing of Environment, 167*, 121-134. doi:10.1016/j.rse.2015.05.004

Dufour, A., Gadallah, F., Wagner, H. H., Guisan, A., & Buttler, A. (2006). Plant species richness and environmental heterogeneity in a mountain landscape: effects of variability and spatial configuration. *Ecography, 29*(4), 573-584. doi:10.1111/j.0906-7590.2006.04605.x

Eisfelder, C., Kuenzer, C., & Dech, S. (2012). Derivation of biomass information for semi-arid areas using remote-sensing data. *International Journal of Remote Sensing, 33*(9), 2937-2984. doi:10.1080/01431161.2011.620034

Fan, F., & Deng, Y. (2014). Enhancing endmember selection in multiple endmember spectral mixture analysis (MESMA) for urban impervious surface area mapping using spectral angle and spectral distance parameters. *International Journal of Applied Earth Observation and Geoinformation, 33*, 290-301. doi:10.1016/j.jag.2014.06.011

Foody, G. M., Muslim, A. M., & Atkinson, P. M. (2005). Super-resolution mapping of the waterline from remotely sensed data. *International Journal of Remote Sensing, 26*(24), 5381-5392. doi:10.1080/01431160500213292

Frazier, A., & Wang, L. (2011). Characterizing spatial patterns of invasive species using sub-pixel classifications. *Remote Sensing of Environment, 115*(8), 1997-2007. doi:10.1016/j.rse.2011.04.002

Gao, B., Montes, M. J., Davis, C. O., & Goetz, A. F. (2009). Atmospheric correction algorithms for hyperspectral remote sensing data of land and ocean. *Remote Sensing of Environment, 113*, S17-S24. doi:10.1016/j.rse.2007.12.015

George, R., Padalia, H., & Kushwaha, S. (2014). Forest tree species discrimination in western Himalaya using EO-1 Hyperion. *International Journal of Applied Earth Observation and Geoinformation, 28*, 140-149. doi:10.1016/j.jag.2013.11.011

Gerten, D., Schaphoff, S., Haberlandt, U., Lucht, W., & Sitch, S. (2004). Terrestrial vegetation and water balance—hydrological evaluation of a dynamic global vegetation model. *Journal of Hydrology, 286*(1-4), 249-270. doi:10.1016/j.jhydrol.2003.09.029

Ghiyamat, A., Shafri, H. Z., Mahdiraji, G. A., Shariff, A. R., & Mansor, S. (2013). Hyperspectral discrimination of tree species with different classifications using single- and multiple-endmember. *International Journal of Applied Earth Observation and Geoinformation, 23*, 177-191. doi:10.1016/j.jag.2013.01.004

Glenn, N. F., Neuenschwander, A., Vierling, L. A., Spaete, L., Li, A., Shinneman, D. J., & Mcilroy, S. K. (2016). Landsat 8 and ICESat-2: Performance and potential synergies for quantifying dryland ecosystem vegetation cover and biomass. *Remote Sensing of Environment, 185*, 233-242. doi:10.1016/j.rse.2016.02.039

Guo, X., Price, K. P., & Stiles, J. (2003). Grasslands Discriminant Analysis Using Landsat TM Single and Multitemporal Data. *Photogrammetric Engineering & Remote Sensing, 69*(11), 1255-1262. doi:10.14358/pers.69.11.1255

Hall, F. G., Hilker, T., Coops, N. C., Lyapustin, A., Huemmrich, K. F., Middleton, E., & Black, T. A. (2008). Multi-angle remote sensing of forest light use efficiency by

observing PRI variation with canopy shadow fraction. *Remote Sensing of Environment, 112*(7), 3201-3211. doi:10.1016/j.rse.2008.03.015

Hestir, E. L., Khanna, S., Andrew, M. E., Santos, M. J., Viers, J. H., Greenberg, J. A., & Ustin, S. L. (2008). Identification of invasive vegetation using hyperspectral remote sensing in the California Delta ecosystem. *Remote Sensing of Environment, 112*(11), 4034-4047. doi:10.1016/j.rse.2008.01.022

Hofer, G., Wagner, H. H., Herzog, F., & Edwards, P. J. (2008). Effects of topographic variability on the scaling of plant species richness in gradient dominated landscapes. *Ecography, 31*(1), 131-139. doi:10.1111/j.2007.0906-7590.05246.x

Keshava, N., & Mustard, J. (2002). Spectral unmixing. *IEEE Signal Processing Magazine, 19*(1), 44-57. doi:10.1109/79.974727

Lee, C. M., Cable, M. L., Hook, S. J., Green, R. O., Ustin, S. L., Mandl, D. J., & Middleton, E. M. (2015). An introduction to the NASA Hyperspectral InfraRed Imager (HyspIRI) mission and preparatory activities. *Remote Sensing of Environment,167*, 6-19. doi:10.1016/j.rse.2015.06.012

Madritch, M. D., Kingdon, C. C., Singh, A., Mock, K. E., Lindroth, R. L., & Townsend, P. A. (2014). Imaging spectroscopy links aspen genotype with below-ground processes at landscape scales. *Philosophical Transactions of the Royal Society B: Biological Sciences, 369*(1643), 20130194-20130194. doi:10.1098/rstb.2013.0194

Marks, D., Seyfried, M., Flerchinger, G., & Winstral, A. (2007). Research Data Collection at the Reynolds Creek Experimental Watershed. Journal of Service Climatology, 1(4), 1-12.

Miller, R. F., & Heyerdahl, E. K. (2008). Fine-scale variation of historical fire regimes in sagebrush-steppe and juniper woodland: an example from California, USA. *International Journal of Wildland Fire,17*(2), 245. doi:10.1071/wf07016

Miller, R. F., Knick, S. T., Pyke, D. A., Meinke, C. W., Hanser, S. E., Wisdom, M. J., & Hild, A. L. (2011). Characteristics of Sagebrush Habitats and Limitations to Long-Term Conservation. *Greater Sage-GrouseEcology and Conservation of a*

Landscape Species and Its Habitats, 144-184. doi:10.1525/california/9780520267114.003.0011

Mitchell, J. J., Shrestha, R., Spaete, L. P., & Glenn, N. F. (2015). Combining airborne hyperspectral and LiDAR data across local sites for upscaling shrubland structural information: Lessons for HyspIRI. *Remote Sensing of Environment, 167*, 98-110. doi:10.1016/j.rse.2015.04.015

Mollot, L. A., Munro, D., & Bilby, R. E. (2007). Classifying fine-scale spatial structure of riparian forests using hyperspectral high-resolution remotely sensed imagery at the Cedar River municipal watershed in western Washington, USA. *Canadian Journal of Remote Sensing,33*(2), 99-108. doi:10.5589/m07-013

NASA Terrestrial Ecology NNX14AD81G

National Research Council. 2002. Riparian Areas: Functions and Strategies for Management. Washington, DC: The National Academies Press. https://doi.org/10.17226/10327

Okin, G. S., Roberts, D. A., Murray, B., & Okin, W. J. (2001). Practical limits on hyperspectral vegetation discrimination in arid and semiarid environments. *Remote Sensing of Environment, 77*(2), 212-225. doi:10.1016/s0034-4257(01)00207-3

Okin, G. S., & Roberts, D. A. (2004). Remote sensing in arid regions: challenges and opportunities.

Ollinger, S. V., Smith, M. L., Martin, M. E., Hallett, R. A., Goodale, C. L., & Aber, J. D. (2002). Regional Variation in Foliar Chemistry and N Cycling among Forests of Diverse History and Composition. *Ecology*, *83*(2), 339. doi:10.2307/2680018

Pan, X., Song, Y., Liu, G., Hu, Y., Ye, X., Cornwell, W. K., & Cornelissen, J. H. (2015). Functional traits drive the contribution of solar radiation to leaf litter decomposition among multiple arid-zone species. *Scientific Reports, 5*(1). doi:10.1038/srep13217

Patten, D. T. (1998). Riparian ecosytems of semi-arid North America: Diversity and human impacts. *Wetlands, 18*(4), 498-512. doi:10.1007/bf03161668

Poulter, B., Frank, D., Ciais, P., Myneni, R. B., Andela, N., Bi, J., & Werf, G. R. (2014). Contribution of semi-arid ecosystems to interannual variability of the global carbon cycle. *Nature, 509*(7502), 600-603. doi:10.1038/nature13376

Pyke, D. A., Chambers, J. C., Pellant, M., Knick, S. T., Miller, R. F., Beck, J. L., & Mciver, J. D. (2015). Restoration handbook for sagebrush steppe ecosystems with emphasis on greater sage-grouse habitat—Part 1. Concepts for understanding and applying restoration. *Circular*. doi:10.3133/cir1416

Qin, W., & Gerstl, S. A. (2000). 3-D Scene Modeling of Semidesert Vegetation Cover and its Radiation Regime. *Remote Sensing of Environment, 74*(1), 145-162. doi:10.1016/s0034-4257(00)00129-2

Reichstein, M., Bahn, M., Ciais, P., Frank, D., Mahecha, M. D., Seneviratne, S. I., & Wattenbach, M. (2013). Climate extremes and the carbon cycle. *Nature, 500*(7462), 287-295. doi:10.1038/nature12350

Richardson, D. M., Holmes, P. M., Esler, K. J., Galatowitsch, S. M., Stromberg, J. C., Kirkman, S. P., & Hobbs, R. J. (2007). Riparian vegetation: degradation, alien plant invasions, and restoration prospects. *Diversity and Distributions, 13*(1), 126-139. doi:10.1111/j.1366-9516.2006.00314.x

Reid, W. V. (2005). Ecosystems and human well-being: synthesis: a report of the Millenium Ecosystems Assessment. Washington, DC: Island Press.

Roberts, D., Gardner, M., Church, R., Ustin, S., Scheer, G., & Green, R. (1998). Mapping Chaparral in the Santa Monica Mountains Using Multiple Endmember Spectral Mixture Models. *Remote Sensing of Environment, 65*(3), 267-279. doi:10.1016/s0034-4257(98)00037-6

Rocchini, D., Mcglinn, D., Ricotta, C., Neteler, M., & Wohlgemuth, T. (2011). Landscape complexity and spatial scale influence the relationship between remotely sensed spectral diversity and survey-based plant species richness. *Journal of Vegetation Science, 22*(4), 688-698. doi:10.1111/j.1654-1103.2010.01250.x

Roth, K. L., Roberts, D. A., Dennison, P. E., Alonzo, M., Peterson, S. H., & Beland, M. (2015). Differentiating plant species within and across diverse ecosystems with imaging spectroscopy. *Remote Sensing of Environment, 167*, 135-151. doi:10.1016/j.rse.2015.05.007

Seyfried, M. S., Harris, R. C., Marks, D., & Jacob, B. (2000). A geographic database for watershed research, Reynolds Creek Experimental Watershed, Idaho, USA. *Tech. Bull. NWRC 2000*, *3*, 26.

Scott, R. L., Biederman, J. A., Hamerlynck, E. P., & Barron-Gafford, G. A. (2015). The carbon balance pivot point of southwestern U.S. semiarid ecosystems: Insights from the 21st century drought. *Journal of Geophysical Research: Biogeosciences, 120*(12), 2612-2624. doi:10.1002/2015jg003181

Shrestha, D. P., Margate, D. E., Anh, H. V., & Van Der Meer, F. (2002). Spectral unmixing versus spectral angle mapper for land degradation assessment: a case study in southern spain. *17th WCSS*, 12-21.

Sibanda, M., Mutanga, O., & Rouget, M. (2016). Discriminating Rangeland Management Practices Using Simulated HyspIRI, Landsat 8 OLI, Sentinel 2 MSI, and VENμS Spectral Data. *IEEE Journal of Selected Topics in Applied Earth Observations and Remote Sensing,9*(9), 3957-3969. doi:10.1109/jstars.2016.2574360

Silván-Cárdenas, J., & Wang, L. (2008). Sub-pixel confusion–uncertainty matrix for assessing soft classifications. *Remote Sensing of Environment, 112*(3), 1081-1095. doi:10.1016/j.rse.2007.07.017

Somers, B., Asner, G. P., Tits, L., & Coppin, P. (2011). Endmember variability in Spectral Mixture Analysis: A review. *Remote Sensing of Environment, 115*(7), 1603-1616. doi:10.1016/j.rse.2011.03.003

Thomey, M. L., Ford, P. L., Reeves, M. C., Finch, D. M., Litvak, M. E., & Collins, S. L. (2014). Review of climate change impacts on future carbon stores and management of warm deserts of the United States. doi:10.2737/rmrs-gtr-316

Thorp, K., French, A., & Rango, A. (2013). Effect of image spatial and spectral characteristics on mapping semi-arid rangeland vegetation using multiple

endmember spectral mixture analysis (MESMA). *Remote Sensing of Environment, 132*, 120-130. doi:10.1016/j.rse.2013.01.008

Wang, H., & Glennie, C. (2015). Fusion of waveform LiDAR data and hyperspectral imagery for land cover classification. *ISPRS Journal of Photogrammetry and Remote Sensing, 108*, 1-11. doi:10.1016/j.isprsjprs.2015.05.012

Wu, J., Wurst, S., & Zhang, X. (2016). Plant functional trait diversity regulates the nonlinear response of productivity to regional climate change in Tibetan alpine grasslands. *Scientific Reports, 6*(1). doi:10.1038/srep35649

Yang, C., Everitt, J. H., & Johnson, H. B. (2009). Applying image transformation and classification techniques to airborne hyperspectral imagery for mapping Ashe juniper infestations. *International Journal of Remote Sensing, 30*(11), 2741-2758. doi:10.1080/01431160802555812

Yi, C., Pendall, E., & Ciais, P. (2015). Focus on extreme events and the carbon cycle. *Environmental Research Letters, 10*(7), 070201. doi:10.1088/1748-9326/10/7/070201

Zare, A., & Ho, K. (2014). Endmember Variability in Hyperspectral Analysis: Addressing Spectral Variability During Spectral Unmixing. *IEEE Signal Processing Magazine, 31*(1), 95-104. doi:10.1109/msp.2013.2279177

CHAPTER FOUR: MONITORING CHANGES IN ABOVEGROUND BIOMASS FROM THE 2015 SODA FIRE

1. Introduction

Wildfires in semi-arid ecosystems have increased in frequency, extent, and severity over the last several decades (Balch et al., 2012; Brooks et al., 2004). The source of these changes is thought to be caused by an increase in drought severity (Yi et al., 2015) and spread of invasive species sparked by current climate change (Brooks et al., 2004; Chambers et al., 2007). Additionally, natural fire cycles have become shorter in duration as a result of anthropogenic causes (Syphard et al., 2009). This increase in fire frequency has changed the composition of native vegetation communities causing a decrease in carbon storage (Bukowski and Baker, 2013; Reichstein et al., 2013) and an increase in post-fire soil erosion (Pierson and Williams, 2016). As wildfire frequency, extent, and severity increase, monitoring the resulting carbon flux becomes a critical issue in understanding the long-term effects on semi-arid ecosystems.

As interest and efforts to monitor carbon flux in post-fire landscapes continue to grow, the issue of scale quickly becomes an important one. Traditional efforts to monitor carbon within a landscape rely on ground crews that gauge the carbon content of streams (Moody et al., 2013), hillslopes (Benavides-Solorio and Macdonald, 2005), and soil (Ravi et al., 2007). Although these efforts provide accurate and detailed insights of the carbon flux within different earth processes, they are limited to small portions of the landscape. Remote sensing offers a unique contribution to understand carbon flux, as airborne and

spaceborne platforms are able to provide landscape coverage. Remote sensing has been widely used to study fire frequency, extent, and severity (Lentile et al., 2006; Keeley, 2009; Eckmann et al., 2009), as well as to monitor vegetation composition and its relationships to biomass and carbon (Eisfelder et al., 2012; Scott et al., 2015; Glenn et al., 2016). Shifting efforts to monitor the health and sustainability of semi-arid ecosystems at the landscape scale using remote sensing will improve fire-driven carbon-flux estimates and their impact on semi-arid ecosystems.

Landsat has been widely used in semi-arid regions to study the effects of fire; specifically, vegetation indices (VI) (both single date and over time) have been used to quantify fire extent (Lentile et al., 2006; Schepers et al., 2014) and burn severity (Keeley 2009; Hardtke et al., 2014). In multi-temporal image analysis, rapid changes in spectral reflectance between pre- and post-fire images are represented with VI that are in turn used to estimate the burn extent and severity (using the amount of vegetation lost as a proxy). Due to the large soil exposure and sparse vegetation in semi-arid ecosystems, traditional indices such as the Normalized Burn Ratio may not be as effective at calculating burn extent in these ecosystems (Norton et al., 2009). Specialized VI, such as the Modified Soil Adjusted Vegetation Index (MSAVI) (Equation 4-1) (Qi et al., 1994), have been developed to help mask the effects of soil and highlight vegetation and thus used to measure burn extent and severity (Rogan and Yool, 2001; Epting et al., 2005; Schepers et al., 2014).

On January 5th, 2015, the United States Secretary of Interior signed Secretarial Order 3336 (SO3336) which was implemented to reduce and prevent wildfires in the western United States, as well as restore sagebrush ecosystems to their natural state.

Specific goals of SO3336 included advancing technology to identify critical areas within the sagebrush steppe, reduce the spread of invasive species, and establish procedures to assess post-fire restoration efforts. The order's mention of utilizing technology to improve current understanding of the state of the sagebrush steppe highlights the importance of using remote sensing to monitor both the pre- and post-fire landscapes. The protocols and data established using remote sensing instruments under SO3336 will provide valuable information about the effects of fire and carbon flux in semi-arid regions.

On August 10th, 2015, the Soda Fire began in Jordan Valley, Oregon, where it burned over 100,000 ha in Oregon and Idaho. Immediately following the Soda Fire, the BLM developed an emergency stabilization and rehabilitation document that detailed a plan to implement a series of restoration efforts over the burned area. Specific objectives of these restoration efforts coincide with those of SO3336 and include restoring vegetation composition to its natural habitat, minimizing the spread of invasive species, and reducing degradation of the post-fire landscape. The motivation and funding for these objectives were provided by SO3336, and hence, the Soda Fire became the order's first case study.

The goal of this study is to provide gross estimates of aboveground biomass (AGB) lost during the 2015 Soda Fire within a portion of Reynolds Creek Experimental Watershed (RCEW) in Southwest Idaho, and relate these estimates to AGB lost over the full extent of the Soda Fire. Additionally, this study provides initial estimates of the spatial distribution of the pre-fire AGB and estimates of post-fire recovery one-year following the fire for RCEW and the full extent of the Soda Fire. The results of this study

offer baseline monitoring information that can be used to further the objectives established by SO3336 and improve our understanding of how wildfire affects carbon flux in the sagebrush steppe at both fine scales (RCEW) and coarser landscape scales (Soda Fire).

Methods

i. Study Area

The study area is Reynolds Creek Experimental Watershed (RCEW), located in southwest Idaho in the Owyhee Mountains and the greater Soda Fire burn extent, which covers portions of Idaho and Oregon (Figure 4-1). Elevation of the RCEW ranges from 900-2100 m with a yearly average precipitation ranging from 250-1100 mm. Environmental conditions within this area have been closely monitored by the United States Department of Agriculture, Agriculture Research service (USDA ARS) since the 1960's (https://www.ars.usda.gov). The RCEW was established as a Critical Zone Observatory (CZO) in 2014 with an overall goal to monitor soil carbon within semi-arid ecosystems, and specifically to understand the factors affecting carbon storage and how this storage varies across the landscape (Lohse et al., 2013). The northern portion of the watershed (7,384 ha) was burned during the 2015 Soda Fire (Figure 4-1). Since then, current research within RCEW has focused on studying the post-fire effects in semi-arid ecosystems. Specific objectives of these studies include quantifying the amount of carbon present in post-fire erosional events. This objective of quantifying carbon and its relationship to AGB along with an extensive history of data collection across the watershed prior to the wildfire makes RCEW an ideal study area.

In this study, we use the burned area within RCEW (~7,400 ha, Figure 4-1) to estimate the amount of AGB that was lost within the watershed. We then extend these estimates to make predictions on the overall total AGB lost to the larger Soda Fire (~113,000 ha, Figure 4-1). A workflow of the methods used during this study is displayed in Figure 4-2.

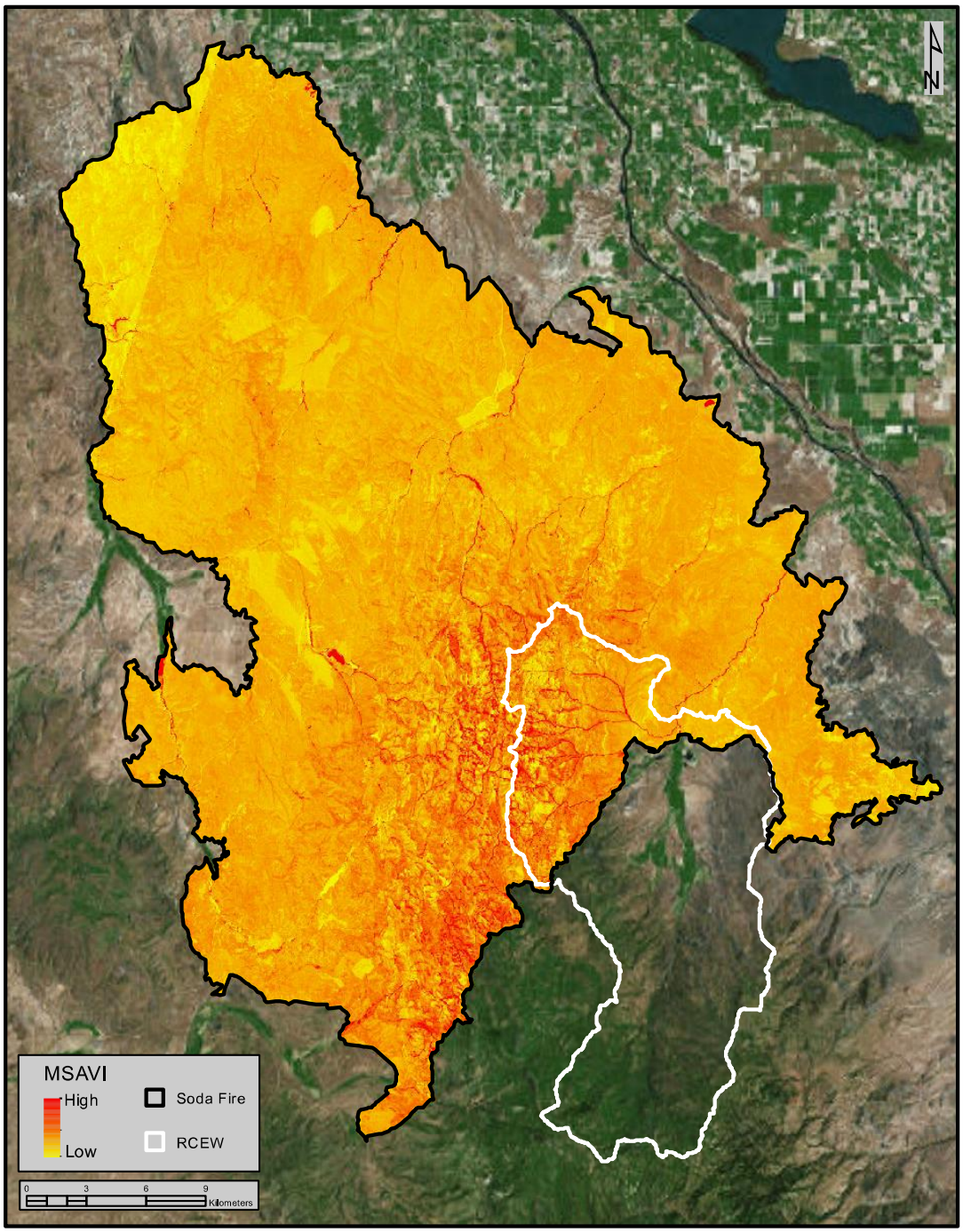

Figure 4-1: Location of Reynolds Creek Experimental Watershed (RCEW) (right) and the Soda Fire burn extent and severity calculated by taking the difference between pre- and post-fire MSAVI (left). Background imagery is National Agriculture Imagery Program (NAIP).

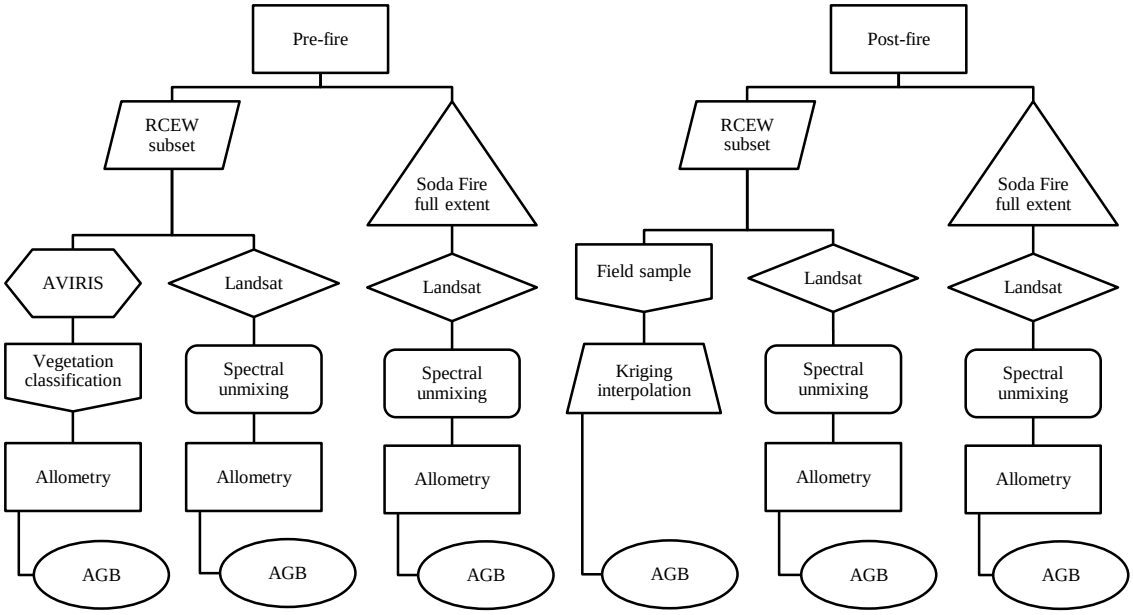

Figure 4-2: Workflow of methods to estimate pre- and post-fire aboveground biomass (AGB).

Multi-Temporal Burn Extent and Severity

We used the Modified Soil Adjusted Vegetation Index (MSAVI, equation 4-1) to calculate the total burn extent of the Soda Fire. Higher differences in MSAVI represent a greater change in vegetation composition and are used as a proxy for burn severity (Epting et al., 2005; Schepers et al., 2014). In this study, burn severity is compared to each pre-fire vegetation class to justify the assumption of total vegetation loss within RCEW during the Soda Fire.

$$MSAVI = \frac{2 * NIR + 1 - \sqrt{(2 * NIR + 1)^2 - 8 * (NIR - RED)}}{2}$$

Equation 4: Modified Soil Adjusted Vegetation Index (MSAVI). NIR = near infrared (~1000 nm), RED = red (~700 nm).

Pre-fire data were collected with Landsat 8 imagery from path 42 row 30 on July 29th, 2015, 12 days prior to the start of the fire. The Landsat imagery was preprocessed to top of the atmosphere reflectance in Exelis Visual Information Solutions (ENVI) version 5.2.1. Due to cloud coverage proceeding the Soda Fire, there were no usable Landsat images covering the burned portion of the study area. However, the EO-1 Advanced Land Imager (ALI) collected an image on August 19th, 2015, and captured the post-fire area. ALI is a multispectral sensor that was developed to mimic Landsat's spatial and spectral resolutions and to be used in replacement for missing temporal data (Lencioni and Hearn, 1997). ALI data were preprocessed in ENVI in the same fashion as the Landsat imagery.

MSAVI was calculated on both the Landsat and ALI imagery within ENVI using the spectral math tool. The difference between the pre- and post-fire MSAVI images was used to calculate the burn extent and burn severity of the Soda Fire based on the amount of change in green vegetation between pre- and post-fire scenes. (Figure 4-1). Burn severity was then classified into low, medium, and high burn severity, where a larger change in vegetation correlated to a higher burn severity.

Pre-fire AGB, RCEW Subset

Classification:

Airborne Visible/Infrared Imaging Spectrometer Next Generation (AVIRIS-ng, or AVIRIS) was collected prior to the Soda Fire on June 11th, 2015 at 1 m spatial resolution. AVIRIS is a hyperspectral sensor that records spectral data from 380-2500 nm at 432 unique values, each approximately 5 nm apart. Imagery was orthorectified, atmospherically corrected, and inspected for noisy bands.

AVIRIS imagery was used to classify vegetation species within RCEW as part of Chapter 3. Vegetation classification of RCEW was divided into two parts due to the complex environmental gradients that span the watershed; species of trees and percent cover of shrubs, grasses, and soil. Dominate tree vegetation that was classified within the watershed consisted of aspen (*Populus termuloides*), Douglas fir (*Psuedotsuga menziesii*), juniper (*Juniperus occidentalis*), and riparian areas (*Populus trichocarpa, Salix exigua*, and *Salix amygdaloides*). Classification had an overall accuracy of 51.2% and a kappa coefficient of 0.38 (Figure 4-3, Table 4-1).

In addition to the vegetation classification stated above, shrub (Artemisia *tridentate* ssp. Wyomingensis, Artemisia *arbuscular*, Ericameria *nauseosa*, and Pushia *tridentate*), grass (*Pseudoroegneria spicata, Hesperostipa comate, and Pascopyrum smithii, Crepis acuminate*), and soil cover within individual pixels was measured using AVIRIS imagery (Figure 4-3). Abundancy estimates were quantified for these classes because they were often characterized by sparse cover that is masked during traditional classification techniques. Cover was derived with a linear spectral unmixing model using the VIPER toolbox (Version 2.0; Roberts et al., 2016). Overall accuracy, kappa coefficient, and user and producer accuracies are shown in Table 4-1.

Vegetation classifications of RCEW were subset to the burned portions of RCEW using the Soda Fire burn extent produced from the Landsat imagery.

Allometry:

A series of allometric equations (Table 4-2) were used to estimate the AGB from the vegetation classifications (Jenkins et al., 2003). These allometric equations were established by relating field measured vegetation characteristics, such as diameter at

breast height (dbh), to destructive samples of AGB for different species of vegetation. Allometry has been used in past studies as a means to provide gross estimates of AGB (Lu 2006; Cleary et al., 2008; Eisfelder et al., 2012). To calculate AGB for tree species, allometric equations require a diameter at breast height (dbh) for individual trees. Since field data of trees within the burned area were not measured prior to the wildfire, average dbh for individual tree species were calculated using United States Department of Agriculture Forest Service's Forest Inventory and Analysis (FIA) data (http://apps.fs.fed.us/fiadb-downloads/datamart.html). FIA data consists of thousands of measurements of individual species across Idaho. A summary of the data, along with average dbh for each tree species used are listed in Table 4-3.

AGB was calculated for each tree class and then scaled up using the total number of pixels for the appropriate classification. Because the allometric equations predict the AGB for individual trees and that trees present were likely larger than the 1 m pixel size of the classification, the use of a 1 m pixel size would severely overestimate AGB. Therefore, to account for this in the allometric equations, estimates were calculated in a 2x2 pixel area. The total number of pixels for each class, excluding shrub and grass, were reduced by a factor of four during this process. A 2x2 pixel area was chosen to represent an average crown diameter between aspen, Douglas Fir, riparian, and juniper classes based on field observations and FIA data. The burn severity map created using the multi-temporal image analysis was compared to the pre-fire vegetation classification map which showed that a majority of each class was located in the highest burn severity portion of the fire. From this observation, it was assumed that all vegetation for the aspen, Douglas Fir, riparian, and juniper classes was consumed within RCEW.

Shrub and grass AGB were estimated using two allometric equations relating percent cover to AGB (Table 4-2) (Mitchell et al., 2017; Dancy et al., 1986). The percent cover for shrub and grass (0 - 100%) from each pixel of the abundancy map was used for these equations. Shrubs are the dominate landcover class for this area and are therefore an important contribution to the total AGB. Shrub and grasses were primarily located in the moderate to low burn severity portions of the fire within RCEW although field observations showed that these regions also had complete consumption of the vegetation that was present. This is likely due to the fact that the burn severity estimates are primarily used for forested ecosystems and often misrepresent shrub ecosystems (Miller and Thode, 2007). Using this knowledge along with the field observations, shrub and grass AGB estimates were also made with the assumption that all pre-fire vegetation was consumed during the fire.

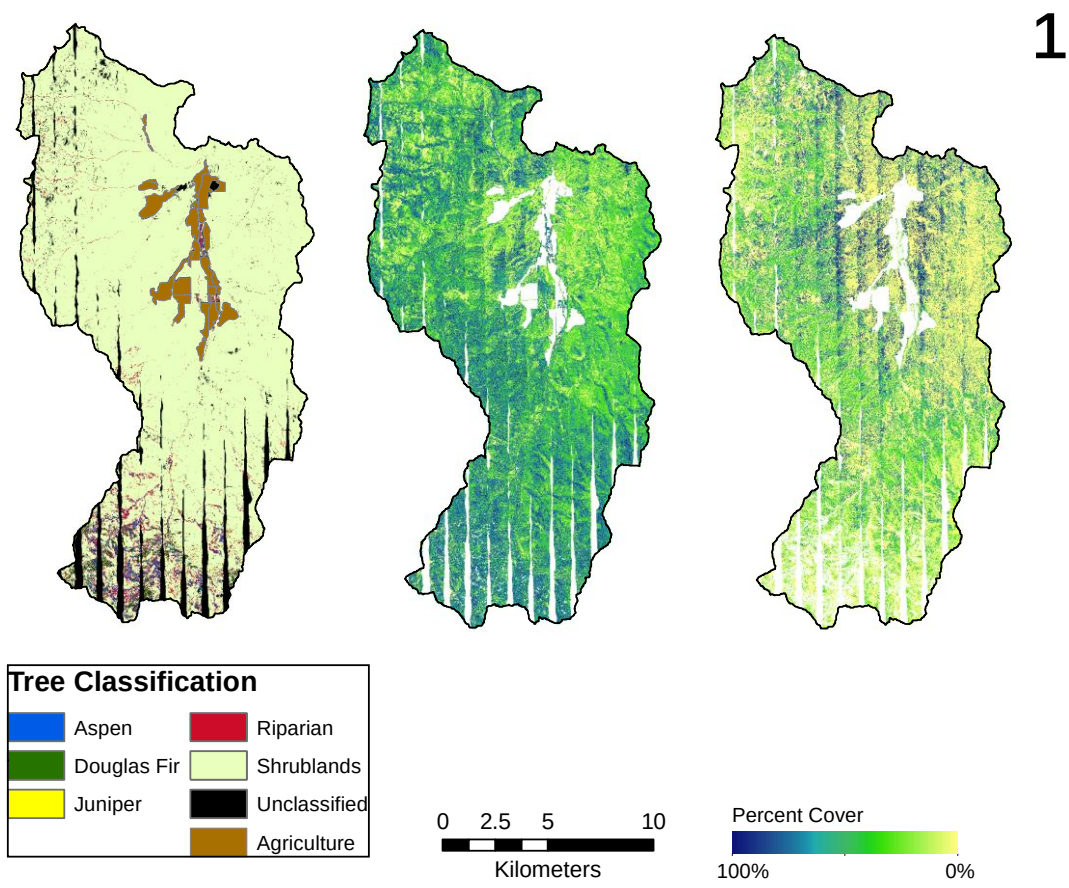

Figure 4-3: Reynolds Creek Experimental Watershed vegetation classification. Tree species classification (left), shrub cover (middle), and grass cover (right). Shrubland class (left) consists of a combination of shrub (middle) and grass (right) cover. Classification accuracy is listed in Table 4-3. Note, black (left) and white (middle and right) strips are caused by missing data between flightlines that occurred during image acquisition.

Table 4-1: Vegetation classification accuracy of Reynolds Creek Experimental Watershed (RCEW).

Tree classification		Abundancy maps		
Overall Accuracy = 51.2% Kappa coefficient = 0.38		Overall Accuracy = 67.4% Kappa coefficient = 0.53		
	Class Accuracy		Producer's Accuracy	User's Accuracy
Riparian	56.2%	Shrubs	98%	48%
Douglas Fir	55.6%	Grass	68%	80%
Juniper	51.5%			
Shrubland	78.8%			

Table 4-2: Allometric equations used to derive aboveground biomass (AGB). Allometric equations for Aspen, Douglas Fir, Juniper, and Riparian relate diameter at breast height (dbh), measured in cm, to AGB, while shrub and grass allometry relate percent cover per one m^2 to AGB.

Vegetation type	Allometric equation	Source
Aspen	$AGB(kg) = e^{(-2.2094 + 2.3867*\ln(dbh(cm))}$	Jenkins et al., 2003
Douglas Fir	$AGB(kg) = e^{(-2.2304 + 2.4435*\ln(dbh(cm))}$	Jenkins et al., 2003
Juniper	$AGB(kg) = e^{(-0.7152+ 1.7029*\ln(dbh(cm))}$	Jenkins et al., 2003
Riparian	$AGB(kg) = e^{(-2.2094 + 2.3867*\ln(dbh(cm))}$	Jenkins et al., 2003
Shrub	$AGB(g)/m^2 = e^{(7.7226 + 1.208*\ln(cover))}/1000$	Mitchell et al., 2017
Grass	$AGB(kg)/m^2 = (e^{((64.1 + cover)/19.4)})/10000$	Dancy et al., 1986

Table 4-3: Summary of the Forest Inventory and Analysis (FIA) data used to derive average diameter at breast height (dbh) used in allometric equations to estimate aboveground biomass

Vegetation type	Number of samples	Average dbh (cm)
Aspen	6,047	15
Douglas Fir	50,077	32
Juniper	1,230	27
Riparian	266	37

Pre-fire AGB, Soda Fire Full Extent

Due to the lack of a pre-fire hyperspectral classification over the entire extent of the Soda Fire, Landsat 8 imagery was used to estimate AGB for the full extent of the Soda Fire. The total abundance of photosynthetic vegetation (PV) was derived from the Landsat imagery using a linear spectral unmixing model (Roberts et al., 1998; Asner and Heidebrecht, 2002; Keshava and Mustard 2002). Gross estimates of total AGB were derived from these abundances using the allometric equation relating shrub cover with AGB (Table 4-2). This equation was chosen because shrub cover was the dominate landcover class of the burned area. No other vegetation classes were considered in the estimate of AGB loss.

Landsat 8 imagery from path 42 row 30 was collected on June 11th, 2015, and pre-processed to top of the atmosphere reflectance in the same process as previously stated. Landsat AGB estimates within RCEW were resampled to 1 m and compared to the total AGB estimates made using the AVIRIS imagery and allometry. Ultimately, abundances and shrub allometry, with the assumption that all vegetation was lost during the wildfire, were used to provide gross estimates of the total AGB lost over the full extent of the Soda Fire.

Spatial Distribution of Pre-Fire AGB, RCEW Subset

A spatial analysis was performed to relate landscape characteristics to vegetation classes and their associated AGB values within the burned area of RCEW. Motivation behind this analysis was to relate AGB loss to landscape parameters that may be correlated with post-fire erosion and vegetation regrowth. A 1 m digital elevation model (DEM) from lidar was used to derive slope degree and aspect. Analysis was performed in ArcMap (version 10.3.1). Relationships for pre-fire vegetation classes within RCEW are presented as the percent of each vegetation class as it relates to a specific landscape characteristic.

Post-fire AGB, RCEW Subset

a) Field data:

A field campaign was performed during May 9-12th, 2016, approximately one year following the Soda Fire. This time of the year was chosen to capture the peak greenness of the area. Field plots 1*1 m in size were randomly selected on the basis that they were in a slope of less than 15 degrees and were within 0.5 km distance from an accessible road. A total of 17 locations were selected across the burned area (Figure 4-4). Samples of the vegetation present were harvested within each plot to obtain an estimate

of the AGB present. The location of the center of each 1*1 m sample was recorded using a Topcon Hiper V Real Time Kinematic (RTK) GPS unit. Samples were dried and weighed to measure AGB (Appendix B).

Additionally, terrestrial lidar was collected at the same locations with a 10*10 m plot design using a Riegl VZ 1000 terrestrial laser scanner (TLS). A large amount of wind caused the grasses to sway during TLS data collection and resulted in noisy data. Therefore, this data was not used for the final analysis but data and results are listed in Appendix B.

Interpolation:

Field measured samples were used to interpolate AGB across the burned area within RCEW using an ordinary kriging approach. Kriging can be broken down into a three-step process: 1) a semivariogram is used to describe the spatial variations observed within a dataset as they relate to distance between samples; 2) a modeled semivariogram is used to approximate the actual dataset in order to describe these spatial variations with a mathematical function; 3) weights used to interpolate an unknown location are determined using the modeled semivariogram (O'Sullivan and Unwin, 2003). An ordinary kriging approach was selected because of its capacity to accurately interpolate surfaces using the underlying relationships that exist between spatial variation of the target variable and the distance between samples (O'Sullivan and Unwin, 2003).

Kriging were performed in ArcMap (version 10.3.1) using the geostatistical analyst toolbox extension. The geostatistical analyst toolbox calculates the semivariogram, uses this to fit a modeled variogram to the dataset, and then performs the

interpolation across the desired area while simultaneously performing a cross-validation using the ground samples to assess the accuracy.

Post-fire AGB, Soda Fire Full Extent:

The abundance of PV and allometry were used to provide gross estimates of one-year post-fire AGB regrowth for the extent of the Soda Fire. The allometric equation relating grass cover to AGB was used for this analysis. Grass allometry was chosen because it was the dominate vegetation observed during the post-fire field campaign. Landsat 8 imagery from path 42 row 30 was collected on May 28th, 2016 and was preprocessed in the same manner as previously stated. This image was chosen because it was cloud free and close to the field campaign. Landsat derived AGB estimates in RCEW were compared to the field AGB estimates within RCEW resulting from the kriging interpolation, and then were used for gross estimates of the full Soda Fire.

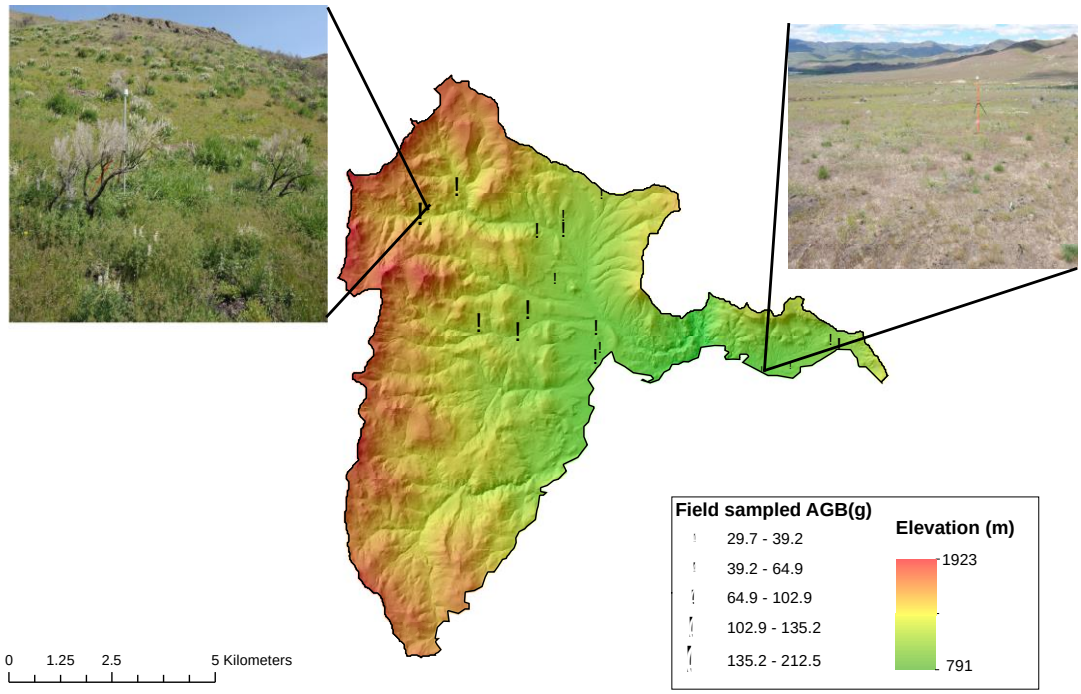

Figure 4-4: Locations of field samples collected in RCEW 1-year following the 2015 Soda Fire. Terrestrial lidar was also collected at each of the sample locations.

Results

i. *AGB Loss from Soda Fire, RCEW Subset and Soda Fire Full Extent*

Total AGB lost within RCEW using the allometric equations indicated approximately 174M kg burned during the Soda Fire (Figure 4-5). Riparian areas had the highest contribution, 71%, of AGB loss, with shrubs, Douglas fir, aspen, juniper, and grass contributing 25%, 3%, 1%, ~0%, and ~0%, respectively (Figure 4-6). Landsat derived AGB loss for RCEW using the PV cover and shrub allometry resampled to 1 m produced significantly lower estimates of approximately 112M kg (Figure 4-5). Landsat derived estimates for the entire extent of the Soda Fire indicated approximately 1.8B kg of AGB lost during the fire.

Spatial Distribution of Pre-fire AGB, RCEW Subset

Results of the spatial distribution of the pre-fire vegetation within RCEW are listed in Tables 4-4 – 4-6. Approximately 70% of the vegetation present within RCEW before the occurrence of the Soda Fire occured on slopes less than 20°, with the majority vegetation concentrated on slopes between 10-20° (Table 4-4). All vegetation classes had their highest abundance on slopes less than 20°.

Northeast facing slopes had the highest percent of vegetation present before the fire with 23%, followed by east, southeast, and north facing slopes, 22%, 15%, and 13%, respectively (Table 4-5). Aspen and riparian had highest concentrations on northeast facing slopes, while all other vegetation classes were primarily on east facing slopes.

One-Year Post-Fire AGB, RCEW Subset and Soda Fire Extent

Total estimates for one-year post-fire regrowth within RCEW produced using the field kriging was approximately 2,100 kg. The resulting map along with its associated standard error is shown in Figure 4-7. Kriging had a root mean square error of 34 g and an average standard error of 28 g.

Landsat derived estimates using the spectral unmixed PV and grass allometry resampled to 1m produced larger estimates of 208,000 kg of AGB regrowth within RCEW. Landsat estimates of total regrowth for the entire Soda Fire indicated approximately 3.2M kg of AGB.

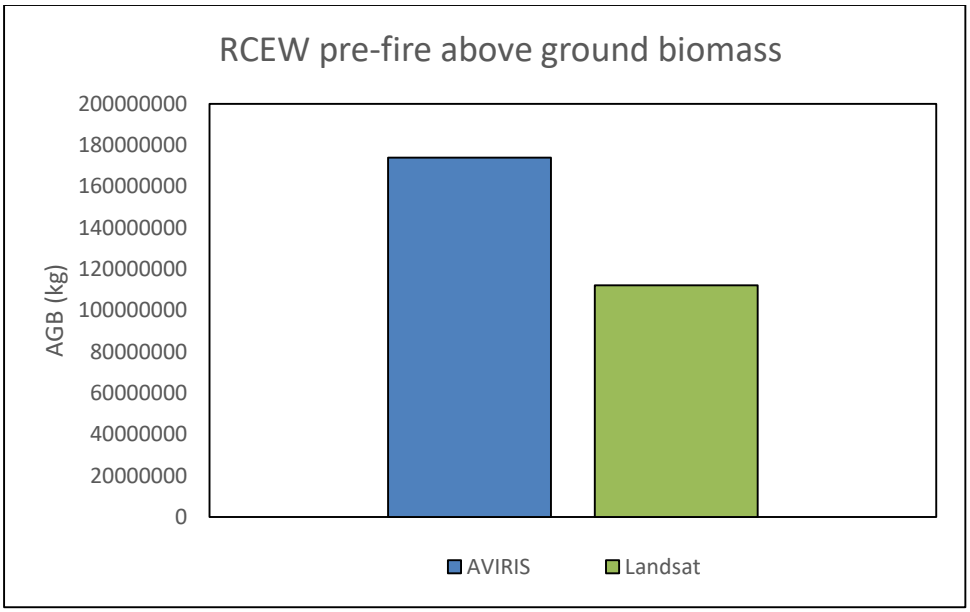

Figure 4-5: Total aboveground biomass lost from the 2015 Soda Fire within the Reynolds Creek Experimental Watershed (RCEW) subset. Both AVIRIS and Landsat resampled to 1 m.

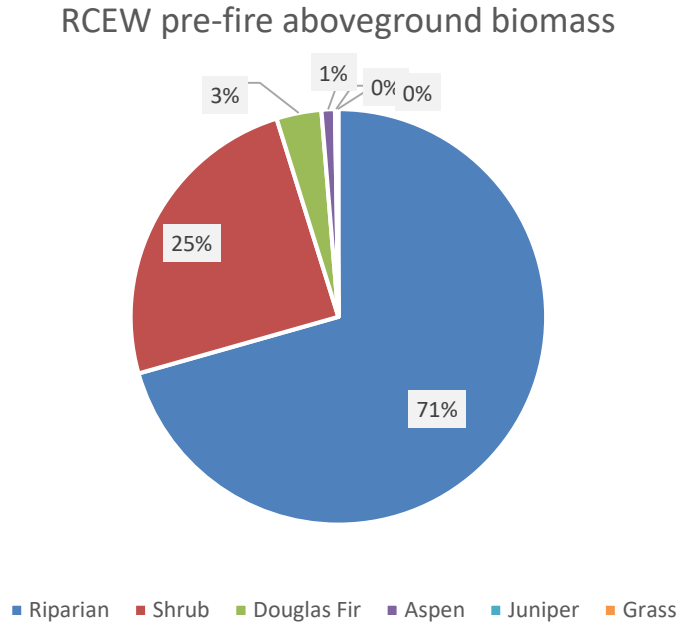

Figure 4-6: Percentage of each vegetation class contributing to the total aboveground biomass loss within the Reynolds Creek Experimental Watershed (RCEW) subset.

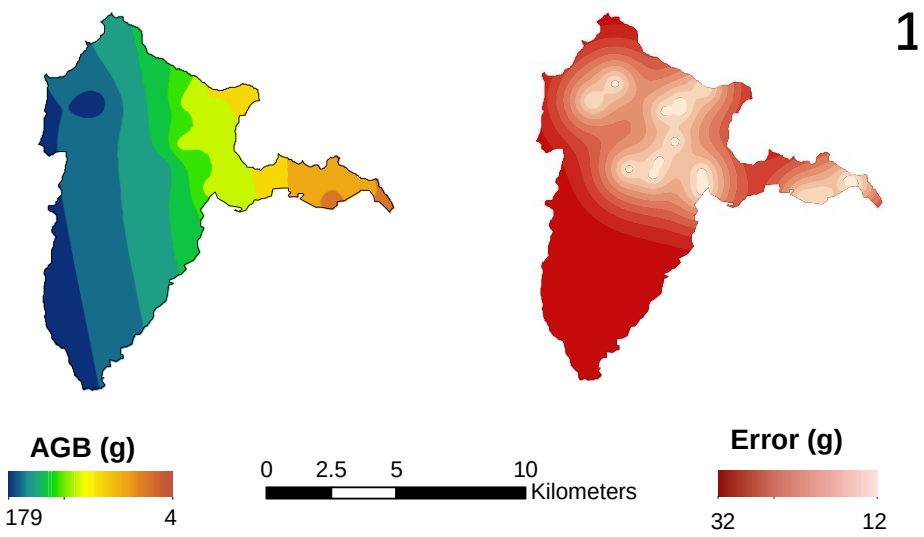

Figure 4-7: Post-fire aboveground biomass (AGB) regrowth within Reynolds Creek Experimental Watershed one-year following the 2015 Soda Fire interpolated with ordinary kriging (left) and its associated error (right).

Table 4-4: The percent of each vegetation class with respect to slope angle in the burned portion of RCEW.

	Slope (degree)					
Vegetation class	0-10	10-20	20-30	30-40	40-50	50-60
Aspen	27	**38**	27	7	1	0
Douglas Fir	**51**	30	14	4	1	0
Juniper	28	**45**	24	3	0	0
Riparian	25	**34**	31	9	1	0
Shrubs	27	**43**	21	4	4	1
RCEW	27	**43**	24	5	1	0

Table 4-5: The percent of each vegetation class present within the burned portion of RCEW, with respect to slope aspect.

Slope aspect	N	NE	E	SE	S	SW	W	NW
Aspen	16	**29**	24	13	8	3	2	5
Douglas Fir	12	17	**20**	18	13	8	6	6
Juniper	9	17	**24**	20	10	5	4	11
Riparian	18	**31**	21	11	8	4	2	5
Shrubs	12	20	**21**	14	10	9	7	7

Discussion

i. AGB Loss

We estimate that approximately 174M kg of AGB was lost within RCEW during the 2015 Soda Fire. This loss includes aspen, Douglas fir, juniper, riparian, shrub, and grass classes. There are several possible errors associated with this estimate, including the assumptions of an average tree crown area of 4 m and the complete consumption of all vegetation during the wildfire. It is noted that there exist trees within RCEW that are both smaller and larger than the 2x2 m area used for estimation and that the burn extent may have been patchy in areas leaving some vegetation unburned. Although these assumptions may have been violated in some areas of RCEW, they applied to a majority of the landscape and any resulting errors are minimal.

Although shrub communities were the largest landcover class, riparian communities contributed the largest loss in biomass within RCEW. The abundancy of water within these regions provides the necessary resources for the occurrence of high-density vegetation, where shrub-dominated areas are often characterized with low AGB. Landsat derived estimates of AGB within RCEW (112M kg) were underestimated when compared to those made with the AVIRIS imagery (174M kg). Landsat derived AGB was likely underestimated because estimates were calculated only using the shrub allometry and the high AGB concentrated within the riparian areas were not accurately represented using this method. This generalization of the landscape's vegetation can only provide us with gross estimates AGB. Future research might consider using a land classification, such as LANDFIRE, in conjunction with the allometry to improve estimates of total AGB loss from the 2015 Soda Fire.

The loss of the two highest contributors to AGB, riparian and shrubs, within RCEW each propose unique challenges to the post-fire landscape. The highest concentration of AGB was located in the channeled riparian areas, where water accumulation and runoff are highest. Previous studies have found that precipitation and runoff are the highest contributors to post-fire erosion of sediment due to reduced infiltration rates and higher flow velocities (Benavides-Solorio and MacDonald, 2005; Moody and Martin, 2009; Moody et al., 2013). Additionally, post-fire sediment within RCEW located on steeper slopes (>20˚) resulting from the pre-fire vegetation located in these areas (~30%) will likely be transported into the channeled areas through runoff or mass wasting events. It is hypothesized that post-fire soil carbon within the eroded sediment will be highest in these channeled regions, and this carbon will be quickly transported out of the system further reducing the total carbon of the post-fire landscape. Quantifying the abundance of carbon present in post-fire erosional events is vital in monitoring fire driven carbon fluxes in semi-arid ecosystems, although there has been a lack of effort in measuring these events in past studies. Together with vegetation biomass loss, the carbon loss from erosion will improve watershed-scale estimates of the total carbon budget.

Shrubs did not have the highest contribution to AGB but they were the largest geographic landcover type in RCEW and over the full extent of the Soda Fire. The large loss of shrub cover over RCEW, and likely over the full extent of the Soda Fire, has important implications to the ecosystem balance within semi-arid regions, as shrubs drive many of the landscape processes (Pyke et al., 2015). For example, shrub canopy cover increases rainfall interception, which mitigates the potential for precipitation-caused

erosion (Pierson and Williams, 2016). Sediment erosion caused by runoff is also increased in post-fire shrub landscapes due to increased connectivity of the post-fire landscape (Lavee et al, 1995; Pierson and Williams, 2016). The loss of shrub cover across the landscape will increase erosion rates leading to a loss of soil, and will create conditions that progress the spread of invasive annual grasses. Growth of invasive grasses such as cheatgrass (*Bromus tectorum*) and goatgrass (*Aegilops spp.*) was observed within RCEW during the post-fire data collection, where the area had received restoration treatments including aerial and drill seeding, and the application of herbicide.

The spatial analysis indicated approximately 58% of all pre-fire vegetation within the RCEW subset was located on north, northeast, and east facing slopes. Previous studies have found that erosion rates, specifically post-fire erosion, are highest on these slope aspects (Moody et al., 2013). This indicates that the post-fire carbon present on these slope aspects will be lost during erosional events more quickly than other slope aspects within RCEW. Since over half of the vegetation consumed during the fire was present on these slope aspects where erosional rates are highest, sediment eroded from these areas will likely have high concentrations of carbon which will be transported either within or out of the system.

AGB Regrowth

We estimate that approximately 2,100 – 208,000 kg of AGB had returned within RCEW one-year following the fire. The large range observed between the field sampled AGB interpolation and Landsat derived estimates is likely a factor of the small sample size of the field plots (n=17). The heterogeneous regrowth of the AGB within RCEW was not fully captured by the field samples which limited the capabilities of the kriging

interpolation. It was estimated that approximately 3.2M kg of AGB returned over the full extent of the Soda Fire in one-year post-fire or only ~ 0.2% of the total pre-fire AGB.

The AGB re-growth shortly following the Soda Fire (~1 year) consisted primarily of grass communities within RCEW. Although cover across the landscape may be high in certain areas, the fundamental composition of AGB and storage of carbon has changed. This composition change has different meanings when related to scale. For example, at the landscape scale the widespread "greenness" from the establishment of post-fire grass communities could be misrepresented as a large abundance or even possible increase in carbon, even though grasses have significantly lower amounts of AGB than shrubs and trees. The lack of AGB becomes increasingly apparent at smaller scales of the landscape. The absence of shrub communities not only lowers the total amount of carbon within the landscape, it also stresses wildlife within the area where shrubs are the main source of food and shelter (Reichstein et al., 2013; Hassan, 2005).

Pre-fire vegetation and environmental characteristics control post-fire vegetation growth, and hence the return of carbon (Kuenzi et al., 2008; Boyd and Davies, 2010; Miller et al., 2013). The abundance of water associated with riparian areas provides the necessary resources needed to reestablish vegetation, and therefore carbon, quickly in the post-fire landscape. The extreme loss of carbon within these areas is not as severe as the loss of carbon in shrub dominated areas because of the quick resilience of this landscape. Previous studies have noted that the reestablishment of shrub cover, specifically sagebrush, varies depending on post-fire landscape and weather conditions, but average recovery time can take 9-50 years following a wildfire (Miller et al., 2013). The increase in fire return intervals and the spread of fire inducing grasses within shrub dominated

areas makes this reestablishment of shrub AGB challenging (Chambers et al., 2007; Balch et al., 2013). Even with the quick return interval of carbon in the riparian areas, the loss of shrub biomass, ~ 25% of the total AGB in RCEW, has large impacts in semi-arid ecosystems. Without the dominate shrub cover across the landscape, the post-fire region will have an overall lower energy balance (Prater and DeLucia, 2006), be more susceptible to the spread of invasive grasses (Chambers et al., 2007), and may not be able to support native wildlife (Aldridge et al., 2008).

Conclusion

The gross estimations of the loss and gain of AGB produced in this study is useful for current research conducted in RCEW that is focused on studying post-fire carbon flux. Remote sensing estimations of AGB offers insight to processes at the landscape scale that cannot be efficiently achieved by ground surveys. As fire extent, severity, and frequency continue to increase in semi-arid ecosystems, monitoring post-fire soil organic carbon transportation will become an important step in understanding global carbon trends.

The estimates produced in this study are also be useful in advancing the goals outlined in SO3336, which calls for long-term monitoring of the recovery of the burned areas in semi-arid ecosystems. This is one of the few studies that has detailed pre-fire vegetation data available at a very fine spatial scale (Kiesecker et al., 2009; Davies et al., 2011; Sanez et al., 2013). The estimates of the AGB burned from different vegetation groups and the AGB returning shortly after the fire provides researchers with baseline information on pre- and post-fire landscape conditions and helps gauge if restoration efforts are effective. Repeat imagery acquired from satellite sensors such as Landsat may

be used to further measure vegetation growth over the burn extent of the Soda Fire. As shrub communities begin to reestablish, there should be an observed decrease in the rapid greenness appearing in the spring months caused by shrub vegetation replacing the widespread grass communities currently present. The availability of this imagery data along with the continuation of long-term ground monitoring of post-fire recovery efforts will provide new insight to help improve strategies to reduce the degrading conditions of semi-arid ecosystems.

References

Aldridge, C. L., Nielsen, S. E., Beyer, H. L., Boyce, M. S., Connelly, J. W., Knick, S. T., & Schroeder, M. A. (2008). Range-wide patterns of greater sage-grouse persistence. *Diversity and Distributions,14*(6), 983-994. doi:10.1111/j.1472-4642.2008.00502.x

Asner, G. P., & Heidebrecht, K. B. (2002). Spectral unmixing of vegetation, soil and dry carbon cover in arid regions: Comparing multispectral and hyperspectral observations. *International Journal of Remote Sensing, 23*(19), 3939-3958. doi:10.1080/01431160110115960

Benavides-Solorio, J. D., & Macdonald, L. H. (2005). Measurement and prediction of post-fire erosion at the hillslope scale, Colorado Front Range. *International Journal of Wildland Fire,14*(4), 457. doi:10.1071/wf05042

Balch, J. K., Bradley, B. A., Dantonio, C. M., & Gómez-Dans, J. (2012). Introduced annual grass increases regional fire activity across the arid western USA (1980-2009). *Global Change Biology, 19*(1), 173-183. doi:10.1111/gcb.12046

Boyd, C. S., & Davies, K. W. (2010). Shrub Microsite Influences Post-Fire Perennial Grass Establishment. *Rangeland Ecology & Management, 63*(2), 248-252. doi:10.2111/rem-d-09-00025.1

Brooks, M. L., Dantonio, C. M., Richardson, D. M., Grace, J. B., Keeley, J. E., Ditomaso, J. M., & Pyke, D. (2004). Effects of Invasive Alien Plants on Fire

Regimes. *BioScience,54*(7), 677. doi:10.1641/0006-3568(2004)054[0677:eoiapo]2.0.co;2

Bukowski, B. E., & Baker, W. L. (2013). Historical fire regimes, reconstructed from land-survey data, led to complexity and fluctuation in sagebrush landscapes. *Ecological Applications, 23*(3), 546-564. doi:10.1890/12-0844.1

Chambers, J. C., Roundy, B. A., Blank, R. R., Meyer, S. E., & Whittaker, A. (2007). What Makes Great Basin Sagebrush Ecosystems Invasible Bybromus Tectorum? *Ecological Monographs, 77*(1), 117-145. doi:10.1890/05-1991

Cleary, M., Pendall, E., & Ewers, B. (2008). Testing sagebrush allometric relationships across three fire chronosequences in Wyoming, USA. *Journal of Arid Environments,72*(4), 285-301. doi:10.1016/j.jaridenv.2007.07.013

Dancy, K. J., Webster, R., & Abel, N. O. J. (1986). Estimating and mapping grass cover and biomass from low-level photographic sampling. *International Journal of Remote Sensing*, *7*(12), 1679-1704.

Davies, K. W., Boyd, C. S., Beck, J. L., Bates, J. D., Svejcar, T. J., & Gregg, M. A. (2011). Saving the sagebrush sea: An ecosystem conservation plan for big sagebrush plant communities. *Biological Conservation, 144*(11), 2573-2584. doi:10.1016/j.biocon.2011.07.016

Eckmann, T. C., Roberts, D. A., & Still, C. J. (2009). Estimating subpixel fire sizes and temperatures from ASTER using multiple endmember spectral mixture analysis. *International Journal of Remote Sensing,30*(22), 5851-5864. doi:10.1080/01431160902748531

Eisfelder, C., Kuenzer, C., & Dech, S. (2012). Derivation of biomass information for semi-arid areas using remote-sensing data. *International Journal of Remote Sensing, 33*(9), 2937-2984. doi:10.1080/01431161.2011.620034

Epting, J., Verbyla, D., & Sorbel, B. (2005). Evaluation of remotely sensed indices for assessing burn severity in interior Alaska using Landsat TM and ETM. *Remote Sensing of Environment,96*(3-4), 328-339. doi:10.1016/j.rse.2005.03.002

Glenn, N. F., Neuenschwander, A., Vierling, L. A., Spaete, L., Li, A., Shinneman, D. J., & Mcilroy, S. K. (2016). Landsat 8 and ICESat-2: Performance and potential synergies for quantifying dryland ecosystem vegetation cover and biomass. *Remote Sensing of Environment, 185*, 233-242. doi:10.1016/j.rse.2016.02.039

Hardtke, L. A., Blanco, P. D., Valle, H. F., Metternicht, G. I., & Sione, W. F. (2015). Semi-automated mapping of burned areas in semi-arid ecosystems using MODIS time-series imagery. International Journal of Applied Earth Observation and Geoinformation, 38, 25-35. doi:10.1016/j.jag.2014.11.011

Hassan, R. (2005). *Ecosystems and human well-being*. Washington, D.C.: Island Press.

Jenkins, J. C., Chojnacky, D. C., Heath, L. S., & Birdsey, R. A. (2003). National-scale biomass estimators for United States tree species. *Forest Science, 49*(1), 12-35.

Keeley, J. E. (2009). Fire intensity, fire severity and burn severity: a brief review and suggested usage. *International Journal of Wildland Fire,18*(1), 116. doi:10.1071/wf07049

Keshava, N., & Mustard, J. (2002). Spectral unmixing. *IEEE Signal Processing Magazine, 19*(1), 44-57. doi:10.1109/79.974727

Kiesecker, J. M., Copeland, H., Pocewicz, A., Nibbelink, N., Mckenney, B., Dahlke, J., & Stroud, D. (2009). A Framework for Implementing Biodiversity Offsets: Selecting Sites and Determining Scale. *BioScience, 59*(1), 77-84. doi:10.1525/bio.2009.59.1.11

Kuenzi, A. M., Fulé, P. Z., & Sieg, C. H. (2008). Effects of fire severity and pre-fire stand treatment on plant community recovery after a large wildfire. *Forest Ecology and Management, 255*(3-4), 855-865. doi:10.1016/j.foreco.2007.10.001

Lavee, H., Kutiel, P., Segev, M., & Benyamini, Y. (1995). Effect of surface roughness on runoff and erosion in a mediterranean ecosystem: the role of fire. Geomorphology, 11(3), 227-234. doi:10.1016/0169-555x(94)00059-z

Lencioni, D. E., & Hearn, D. R. (1997). New Millennium EO-1 Advanced Land Imager. In *International Symposium on Spectral Sensing Research*. 13-19.

Lentile, L. B., Holden, Z. A., Smith, A. M., Falkowski, M. J., Hudak, A. T., Morgan, P., & Benson, N. C. (2006). Remote sensing techniques to assess active fire characteristics and post-fire effects. *International Journal of Wildland Fire,15*(3), 319. doi:10.1071/wf05097

Lohse, KA, M Seyfried, A Flores, S Benner, N Glenn. (2013): Reynolds Creek Carbon Critical Zone Observatory. NSF Proposal.

Lu, D. (2006). The potential and challenge of remote sensing-based biomass estimation. *International Journal of Remote Sensing,27*(7), 1297-1328. doi:10.1080/01431160500486732

Miller, R. F., Chambers, J. C., Pyke, D. A., Pierson, F. B., & Williams, C. J. (2013). A review of fire effects on vegetation and soils in the Great Basin Region: response and ecological site characteristics. doi:10.2737/rmrs-gtr-308

Miller, J. D., & Thode, A. E. (2007). Quantifying burn severity in a heterogeneous landscape with a relative version of the delta Normalized Burn Ratio (dNBR). *Remote Sensing of Environment, 109*(1), 66-80. doi:10.1016/j.rse.2006.12.006

Mitchell, J., Poley, A., Maloney, M., Ilangakoon, N., Dashti, H., Qi, Y., Ustin, S., Glann, N. (2017). Toward regional shrub biomass and uncertainty mapping in the western US using airborne lidar and imaging spectroscopy , SilviLaser 2017, Blacksburg, VA.

Moody, J. A., & Martin, D. A. (2009). Synthesis of sediment yields after wildland fire in different rainfall regimes in the western United States. *International Journal of Wildland Fire,18*(1), 96. doi:10.1071/wf07162

Moody, J. A., Shakesby, R. A., Robichaud, P. R., Cannon, S. H., & Martin, D. A. (2013). Current research issues related to post-wildfire runoff and erosion processes. *Earth-Science Reviews,122*, 10-37. doi:10.1016/j.earscirev.2013.03.004

Norton, J., Glenn, N., Germino, M., Weber, K., & Seefeldt, S. (2009). Relative suitability of indices derived from Landsat ETM and SPOT 5 for detecting fire severity in

sagebrush steppe. *International Journal of Applied Earth Observation and Geoinformation,11*(5), 360-367. doi:10.1016/j.jag.2009.06.005

O'sullivan, D., & Unwin, D. (2014). *Geographic information analysis*. John Wiley & Sons.

Pierson, F. B., & Williams, C. J. (2016). Ecohydrologic impacts of rangeland fire on runoff and erosion: A literature synthesis.

Prater, M. R., & Delucia, E. H. (2006). Non-native grasses alter evapotranspiration and energy balance in Great Basin sagebrush communities. *Agricultural and Forest Meteorology,139*(1-2), 154-163. doi:10.1016/j.agrformet.2006.08.014

Pyke, D. A., Chambers, J. C., Pellant, M., Knick, S. T., Miller, R. F., Beck, J. L., & Mciver, J. D. (2015). Restoration handbook for sagebrush steppe ecosystems with emphasis on greater sage-grouse habitat—Part 1. Concepts for understanding and applying restoration. *Circular*. doi:10.3133/cir1416

Qi, J., Chehbouni, A., Huete, A. R., Kerr, Y. H., & Sorooshian, S. (1994). A modified soil adjusted vegetation index. *Remote sensing of environment, 48*(2), 119-126.

Ravi, S., Dodorico, P., Zobeck, T. M., Over, T. M., & Collins, S. L. (2007). Feedbacks between fires and wind erosion in heterogeneous arid lands. *Journal of Geophysical Research: Biogeosciences,112*(G4). doi:10.1029/2007jg000474

Reichstein, M., Bahn, M., Ciais, P., Frank, D., Mahecha, M. D., Seneviratne, S. I., & Wattenbach, M. (2013). Climate extremes and the carbon cycle. *Nature, 500*(7462), 287-295. doi:10.1038/nature12350

Roberts, D., Gardner, M., Church, R., Ustin, S., Scheer, G., & Green, R. (1998). Mapping Chaparral in the Santa Monica Mountains Using Multiple Endmember Spectral Mixture Models. *Remote Sensing of Environment, 65*(3), 267-279. doi:10.1016/s0034-4257(98)00037-6

Rogan, J., & Yool, S. R. (2001). Mapping fire-induced vegetation depletion in the Peloncillo Mountains, Arizona and New Mexico. *International Journal of Remote Sensing,22*(16), 3101-3121. doi:10.1080/01431160152558279

Saenz, S., Walschburger, T., González, J. C., León, J., Mckenney, B., & Kiesecker, J. (2013). Development by Design in Colombia: Making Mitigation Decisions Consistent with Conservation Outcomes. *PLoS ONE, 8*(12). doi:10.1371/journal.pone.0081831

Schepers, L., Haest, B., Veraverbeke, S., Spanhove, T., Borre, J. V., & Goossens, R. (2014). Burned Area Detection and Burn Severity Assessment of a Heathland Fire in Belgium Using Airborne Imaging Spectroscopy (APEX). *Remote Sensing,6*(3), 1803-1826. doi:10.3390/rs6031803

Scott, R. L., Biederman, J. A., Hamerlynck, E. P., & Barron-Gafford, G. A. (2015). The carbon balance pivot point of southwestern U.S. semiarid ecosystems: Insights from the 21st century drought. *Journal of Geophysical Research: Biogeosciences, 120*(12), 2612-2624. doi:10.1002/2015jg003181

Syphard, A. D., Radeloff, V. C., Hawbaker, T. J., & Stewart, S. I. (2009). Conservation Threats Due to Human-Caused Increases in Fire Frequency in Mediterranean-Climate Ecosystems. Conservation Biology, 23(3), 758-769. doi:10.1111/j.1523-1739.2009.01223.x

Yi, C., Pendall, E., & Ciais, P. (2015). Focus on extreme events and the carbon cycle. *Environmental Research Letters, 10*(7), 070201. doi:10.1088/1748-9326/10/7/070201

CHAPTER FIVE: CONCLUSION

This thesis was focused on deriving high spatial resolution vegetation cover and aboveground biomass in a semi-arid ecosystem. The two studies conducted within this thesis use remote sensing to capture this information at a landscape scale. Currently high resolution (1 m) hyperspectral data is rare which has hindered the development of new strategies to preserve semi-arid ecosystems in the Western United States. As data become more widely available from future satellite missions, such as NASA's hyperspectral sensor HyspIRI, scientist and government officials can improve current conservation and restoration methods to ensure the long-term preservation of these ecosystems.

The first manuscript provided a detailed assessment of the ability of high spatial resolution hyperspectral imagery to classify vegetation across large environmental gradients and ecotones. The study site was Reynolds Creek Experimental Watershed (RCEW) in southwest Idaho and consisted of 23,900 ha of semi-arid ecosystem. The resulting products from this study include: a 1 m classification of vegetation species (Aspen, Douglas Fir, Juniper, and Riparian), a 1 m classification of plant functional types (deciduous, evergreen, and shrublands), and 1 m abundancy maps of shrub, grass, and soil cover. The accuracy of each of these products was assessed and reported using *in-situ* vegetation data collected across the watershed.

The second manuscript focused on using the classification produced in the first study to provide detailed estimates of aboveground biomass (AGB) loss within RCEW from the 2015 Soda Fire and relate this information to develop estimates of AGB loss over

the full extent of the Soda Fire derived from Landsat imagery. AGB estimates showed approximately 174M kg was lost within RCEW and 1.8B kg was lost over the full extent of the Soda Fire. This study also provided rough estimates of the amount of AGB that returned to the burned landscape one-year following the fire. Analysis showed approximately 208,000 kg of AGB had returned within RCEW and 3.2M kg over the full Soda Fire extent.

Future research to continue the work from this thesis could focus on the effects of the 2015 Soda Fire and monitoring vegetation recovery in subsequent years. Estimates of vegetation composition and AGB produced in this work can be used as baseline information that can be used to estimate carbon post-fire abundances, assess restoration efforts, and track vegetation recovery rates. Specific scientific questions of interest to future researchers may include quantifying the amount of soil carbon present within post-fire erosional events, monitoring how vegetation composition changes with areas that received different restoration treatments compared to the pre-fire vegetation conditions, and monitoring the recovery rates of AGB and carbon across the entire burned landscape.

These questions will help fill a knowledge gap that exists in post-fire recovery and carbon flux that larger studies, such as those being conducted by the Critical Zone Observatory and under Secretarial Order 3336, are focused on. As semi-arid ecosystems continue to degrade, monitoring vegetation health will be vital in long-term preservation of the landscape.

APPENDIX A

A. Reynolds Creek Experimental Watershed field plots.

Plot	Year	Dominant vegetation	Shrub cover	Grass cover	Soil cover
1	2014	Bitterbrush	47	37	16
2	2014	Bitterbrush	78	21	1
3	2014	Bitterbrush	30	65	5
4	2014	Bitterbrush	43	49	8
5	2014	Bitterbrush	60	34	6
6	2014	Bitterbrush	64	35	1
7	2014	Bitterbrush	64	35	1
8	2014	Bitterbrush	59	40	1
9	2014	Bitterbrush	35	30	35
10	2014	Bitterbrush	36	35	29
11	2014	Sagebrush	45	34	21
12	2014	Sagebrush	37	33	30
13	2014	Sagebrush	36	36	28
14	2014	Sagebrush	46	33	21
15	2014	Sagebrush	40	18	42
16	2014	Sagebrush	31	42	27
17	2014	Sagebrush	33	2	65
18	2014	Sagebrush	61	9	30
19	2014	Sagebrush	48	11	41
20	2014	Sagebrush	75	5	20
21	2014	Rabbitbrush	71	8	21
22	2014	Mixed	5	60	35
23	2014	Mixed	62	36	2
24	2014	Grass	34	3	63
25	2015	Sagebrush	27	34	39
26	2015	Sagebrush	13	17	70
27	2015	Sagebrush	18	58	24
28	2015	Sagebrush	64	24	12
29	2015	Sagebrush	28	18	54
30	2015	Sagebrush	77	0	23
31	2015	Sagebrush	88	4	8
32	2015	Sagebrush	33	57	10
33	2015	Sagebrush	62	29	9
34	2015	Sagebrush	79	20	1
35	2015	Sagebrush	55	32	13
36	2015	Sagebrush	49	46	5
37	2015	Sagebrush	66	1	33
38	2015	Sagebrush	53	23	24
39	2015	Sagebrush	59	29	12
Plot	Year	Dominant vegetation	Shrub cover	Grass cover	Soil cover
40	2015	Sagebrush	48	35	17
41	2015	Sagebrush	32	34	34
42	2015	Sagebrush	23	43	34
43	2015	Rabbitbrush	43	47	10

44	2015	Mixed	36	47	17
45	2015	Mixed	26	45	29
46	2015	Mixed	27	72	1
47	2015	Mixed	58	42	0
48	2015	Grass	36	61	3

APPENDIX B

B. One-year post-fire aboveground biomass within a subset of Reynolds Creek Experimental Watershed derived with terrestrial lidar scanning.

Plot number	Field sampled dry weight (g)	TLS AGB (g)	Aerial seeded	Drill Seeded
1	59.59	NA	Yes	Yes
2	49.58	NA	Yes	Yes
3	88.18	150,500	Yes	Yes
4	85.69	106,196	Yes	Yes
5	51.19	NA	Yes	Yes
6	212.49	22,268	Yes	No
7	124.5	30,988	Yes	No
8	102.94	33,828	Yes	No
9	56.9	61,036	Yes	No
10	89.53	105,976	Yes	Yes
11	135.21	54,496	Yes	No
12	130.69	68,728	Yes	Yes
13	85.99	NA	Yes	No
14	64.88	121,984	Yes	No
15	29.66	126,688	Yes	No
16	39.24	128,316	Yes	No
17	122.75	101,816	Yes	No